MODELING AND ANALYSIS OF THZ COMMUNICATION SYSTEMS

M.Tech. Thesis

By

VAISHALI ROHILLA

DEPARTMENT OF ELECTRICAL ENGINEERING

INDIAN INSTITUTE OF TECHNOLOGY INDORE

MAY 2025

MODELING AND ANALYSIS OF THZ COMMUNICATION SYSTEMS

A THESIS

Submitted in partial fulfillment of the
requirements for the award of the degree
of

Master of Technology

by

VAISHALI ROHILLA

DEPARTMENT OF ELECTRICAL ENGINEERING
INDIAN INSTITUTE OF TECHNOLOGY INDORE

MAY 2025

INDIAN INSTITUTE OF TECHNOLOGY INDORE

CANDIDATE'S DECLARATION

I hereby certify that the work which is being presented in the thesis entitled **MODELING AND ANALYSIS OF THZ COMMUNICATION SYSTEMS** in the partial fulfillment of the requirements for the award of the degree of **MASTER OF TECHNOLOGY** and submitted in the **DEPARTMENT OF ELECTRICAL ENGINEERING**, Indian Institute of Technology Indore, is an authentic record of my own work carried out during the time period from **JUNE 2023** to **May 2025** under the supervision of **Dr. Swaminathan Ramabadran, Assistant Professor at Indian Institute of Technology Indore**.

The matter presented in this thesis has not been submitted by me for the award of any other degree of this or any other institute.

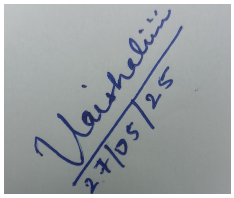

Signature of the student with date

(VAISHALI ROHILLA)

. . . . . .

This is to certify that the above statement made by the candidate is correct to the best of my/our knowledge.

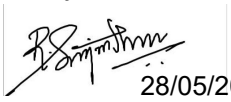

28/05/2025

Signature of the Supervisor of

M.Tech. thesis(with date)

(Dr. SWAMINATHAN RAMABADRAN)

. . . . . .

VAISHALI ROHILLA has successfully given his/her M.Tech. Oral Examination held on 07/05/2025.

Signature(s) of Supervisor(s)

Date: 28/05/2025

Saptarshi Ghosh

Convener, DPGC

Date: 04-06-2025

Chapter 1

Acknowledgments

First and foremost, I would like to express my deepest gratitude to my supervisor, Dr. Swaminathan Ramabadran for his exceptional guidance and perennial support throughout the entire duration of my research. I am grateful for Dr. Swaminathan Ramabadran's patience and willingness to engage in thorough discussions that in turn has cleared my concepts and helped me expand my horizons as a researcher. His dedication as well as way of doing research has inspired and motivated me to pursue excellence in my future research. I consider myself fortunate to have had the opportunity to work under his supervision.

I am indebted to Mr. Prashant Sharma for providing me with the invaluable advises, knowledge, skills, and opportunities necessary for my growth as a researcher throughout my time in the lab. I would also like to thank my other colleagues at lab Mr. Manoj Khokare, Mr. Nayim Ahmed, Mr. Kishan Tripathi, and Mr. M Sai Vamshi for the camaraderie and positive energy that they brought to the lab everyday.

I sincerely acknowledge IIT Indore and Ministry of Education (MoE), Govt. of India, for supporting my M.Tech. by providing lab facilities and TA scholarship, respectively.

My work would not have been possible without the encouragement of my parents, whose tremendous support helped me stay positive and overcome the worst of hurdles. To them, I will forever be grateful.

Last but not the least, I offer my reverence onto the lotus feet of Lord Krishna for his divine blessings.

Abstract

In this thesis we propose multi-Relay dual-hop terahertz communication systems and multi-IRS assisted terahertz communication systems.

With the imminent rollout of sixth-generation (6G) and beyond wireless networks, Terahertz (THz) communication is emerging as a cornerstone for addressing the rapidly growing demands of high-speed data, ultra-reliable low-latency communication (URLLC), and massive machine-type communication (mMTC). Operating in the 0.1–10 THz frequency range, THz bands offer unprecedented spectrum availability, enabling ultra-high throughput and secure transmissions. However, the propagation characteristics at these frequencies pose significant challenges, including severe path loss, atmospheric absorption, molecular scattering, and beam misalignment—making direct, long-distance THz communication highly unreliable.

This thesis addresses these issues by proposing and analyzing two distinct yet complementary system models: (i) **multi-relay-enhanced dual-hop THz communication systems** and (ii) **multi-IRS-assisted THz communication systems**. Both approaches aim to improve signal robustness, link reliability, and coverage in high-frequency environments.

In the first part of the thesis, a multi-relay dual-hop THz communication system employing Decode-and-Forward (DF) relays and an Opportunistic Relay Selection (ORS) scheme is considered. The underlying channels are modeled using generalized α–μ fading with pointing errors to capture real-world impairments. Closed-form expressions for outage probability, average symbol error rate (SER), and ergodic capacity are derived. Asymptotic analyses are performed to evaluate diversity gains at high signal-to-noise ratios (SNR). Monte Carlo simulations validate the analytical results, confirming that increasing the number of relays enhances diversity and system performance.

The second part of the work investigates a multi-Intelligent Reflecting Surface (IRS)-assisted THz system. IRSs are passive, reconfigurable metasurfaces that manipulate elec-

tromagnetic wave propagation by inducing phase shifts, thus enabling virtual line-of-sight (LoS) paths. Unlike relays, IRSs do not introduce additional noise or power consumption. The proposed system leverages multiple IRSs and elements per surface to create composite LoS paths around obstacles. End-to-end performance metrics such as outage probability, SER, and ergodic capacity are analyzed using statistical tools including multivariate Fox's H-function. Asymptotic expressions reveal that increasing the number of IRSs and reflecting elements significantly boosts diversity gain and improves overall system reliability. Simulation results align closely with the theoretical expressions and validate the robustness of the proposed model.

Comparative analysis reveals that while both multi-relay and multi-IRS schemes offer substantial performance gains, IRSs present a more scalable and energy-efficient alternative, especially suitable for dense, indoor, or urban environments where power and hardware complexity are critical concerns. However, relays provide stronger gains in severely blocked or highly dynamic environments due to their active regeneration capabilities.

Overall, this thesis contributes to the theoretical modeling and performance evaluation of advanced THz communication systems under realistic conditions. The work highlights critical design parameters and offers valuable insights into deploying cooperative and reconfigurable technologies for future wireless networks.

Contents

Chapter 2

Introduction

2.1 Background

The exponential growth of data-intensive wireless applications—such as ultra-high-definition video streaming, augmented reality (AR), virtual reality (VR), and autonomous vehicle communication—has placed unprecedented demands on wireless networks. Fifth-generation (5G) wireless systems, although a significant leap from their predecessors, still fall short in key performance areas required for next-generation connectivity. Operating primarily in the sub-6 GHz and millimeter-wave (mmWave) bands, 5G systems face severe challenges such as limited available bandwidth, high latency in ultra-dense deployments, reduced spectral efficiency under mobility, and signal degradation due to blockage and penetration losses. The mmWave bands offer wider bandwidth compared to traditional bands, yet are heavily constrained by high path loss and poor diffraction properties. These shortcomings highlight the need for a more advanced wireless communication paradigm to meet the envisioned goals of higher data rates, ultra-low latency, enhanced spectral efficiency, and reliable connectivity in diverse propagation environments.

Sixth-generation (6G) wireless communication has emerged as a transformative vision to address these limitations, with Terahertz (THz) frequency bands (0.1–10 THz) considered a key enabler. THz bands offer vast unused spectral resources, which can support data rates on the order of terabits per second (Tbps), fulfilling the high-throughput and low-latency requirements of future applications. However, THz waves experience severe free-space path loss, molecular absorption, and limited diffraction, making them highly sensitive to blockages and predominantly suitable for short-range, line-of-sight (LoS) communications. These

propagation challenges significantly limit the effectiveness and coverage of standalone THz communication links, especially in indoor or dense urban environments with frequent non-line-of-sight (NLoS) conditions.

To overcome these constraints, cooperative communication techniques such as Decode-and-Forward (DF) relaying and Intelligent Reflecting Surfaces (IRSs) have been proposed. In DF relaying, intermediate nodes receive the transmitted signal, decode it, and then forward a re-encoded version to the destination. This method provides a reliable means of extending communication range, enhancing link quality, and improving system robustness in harsh THz environments. By strategically placing DF relays, especially in NLoS regions or behind obstacles, the coverage area of THz communication can be effectively expanded, enabling reliable connectivity beyond the LoS region.

On the other hand, IRSs are passive, reconfigurable metasurfaces composed of numerous reflecting elements that can manipulate incident electromagnetic waves to enhance signal propagation. In this work, we consider IRSs without explicit modeling of phase shift optimization, focusing instead on their spatial signal reflection capability to construct favorable propagation paths. IRSs can create virtual LoS links around obstacles, improving received signal strength in challenging environments. They offer an energy-efficient alternative to active relays, since they do not introduce additional noise or require high power consumption, and can be seamlessly integrated into existing environments like building facades or indoor walls.

While single-relay or single-IRS-assisted systems offer performance improvements, their capabilities are inherently limited in dynamic or highly obstructed scenarios. This has led to growing interest in multi-relay and multi-IRS-assisted communication systems, particularly for THz networks. Deploying multiple DF relays enables diversity gain, providing multiple independent paths from source to destination, which can significantly improve outage probability, bit error rate, and overall link reliability. Likewise, multi-IRS systems can enhance the reflected signal paths through different spatial configurations, resulting in increased diversity gain and improved signal coverage, especially in environments with high variability and obstacles.

2.2 Literature Review

Recent advancements in THz communication have focused on addressing key propagation challenges—such as severe path loss, limited diffraction, and atmospheric absorption—by introducing cooperative strategies like decode-and-forward (DF) relaying and reconfigurable intelligent surfaces (RISs), which are emerging as promising enablers for next-generation wireless networks. These techniques not only extend communication range but also enhance link robustness and diversity gain in both standalone and hybrid THz/FSO systems.

In the context of relaying, DF-based multi-relay based systems have demonstrated significant performance gains under fading and misalignment conditions. A dual-hop THz system employing DF relays and opportunistic relay selection (ORS) was investigated, where closed-form expressions for outage probability, average symbol error rate (SER), and ergodic capacity were derived under α–μ fading and pointing errors. This work established the diversity benefits of relay-assisted THz communication. Similar enhancements were reported in [1], where a dual-hop THz-RF system was analyzed, and relaying was shown to mitigate performance degradation from atmospheric turbulence and molecular absorption. Furthermore, beam misalignment, which can critically affect THz links, was explicitly addressed in [2] by modeling stochastic pointing errors and incorporating relays to ensure signal robustness.

Relaying techniques have also been extended to multi-hop configurations. In [3], a multi-hop THz wireless system was studied under mixed fading and shadowing effects, showing how intermediate DF relays can support longer distance communication by compensating for fading and absorption losses. Works such as [4] further evaluated DF and fixed-gain relaying under fading models like Rayleigh and α–μ, highlighting that DF relays can eliminate noise at intermediate hops, unlike amplify-and-forward (AF) counterparts, which amplify noise along with the signal.

Beyond relay-only systems, a new class of solutions incorporates RISs to reconfigure the wireless environment and passively enhance signal quality. RIS technology enables reflection of incident waves with controlled phase shifts to construct virtual LoS paths. In [5], the use of RISs in a THz-OFDM-MIMO system was found to significantly boost SNR and mitigate path blockages. Further performance improvements were observed in [6], where RIS-assisted THz systems under α–μ fading and hardware imperfections were studied, showing

effective control over signal strength without active power consumption.

In hybrid architectures, RISs have been shown to complement relay systems effectively. For example, in [7], a mixed THz/FSO system was enhanced by incorporating RISs at both links, enabling performance resilience against fog, misalignment, and atmospheric turbulence. This system used a DF relay to bridge the THz and FSO domains, and performance metrics such as outage probability and average bit error rate (ABER) were derived using advanced Fox's H-function modeling. Similarly, [8] presented a RIS-aided hybrid FSO/THz system using MRC and SC diversity techniques, showing improved reliability under non-LoS conditions.

RIS integration has also been extended to mobile platforms. In [9], a UAV-assisted RIS relay for FSO/THz links was analyzed, offering mobility-aware beam reconfiguration to overcome LoS obstructions in dynamic scenarios. In parallel, [10]explored RIS-empowered optical links and modeled statistical turbulence and misalignment effects, providing a more complete analysis of channel behavior in real-world deployments.

Hybrid relaying systems involving THz and RF were also explored in [11], where THz was used as a primary link with RF as a backup via DF relays, showing reduced outage in rain-fading scenarios. The integration of RIS in RF/FSO systems was further studied in [12], indicating that RIS can substitute for active relays in certain conditions while maintaining high SNR levels and extending communication range.

Advancements in relay optimization were also reported in [13] and [14], which addressed the use of multi-hop and full-duplex DF relaying over generalized fading channels, demonstrating spectral efficiency gains and robustness to channel variation. Analytical frameworks provided in these works guided the selection of optimal relay numbers and placement strategies to maximize diversity gain.

Unified performance analysis for relay-assisted and RIS-based systems has also gained attention. In [15], a generalized analytical model for MIMO RF/FSO systems was developed, accounting for channel impairments and hardware limitations, while [16] proposed a unified framework for evaluating outage probability in dual-hop DF systems under mixed fading conditions.

Collectively, these studies demonstrate that DF relaying actively regenerates signals across long distances, mitigating signal degradation due to fading and blockages, while RIS provides a passive, energy-efficient alternative for enhancing signal strength and re-

routing propagation around obstacles. When combined in hybrid configurations, especially with multi-relay and multi-RIS deployment, these techniques offer robust, high-capacity, and low-latency solutions critical for practical deployment of THz-enabled 6G systems.

2.3 Motivations and Contributions

2.3.1 Chapter 2

The motivations behind the work in Chapter 2 are summarized as follows:

1. The THz band suffers from severe path loss, atmospheric absorption, and misalignment issues.

2. Existing THz systems are constrained by short transmission ranges due to LoS dependency and fading, which motivates the use of relaying techniques to enhance coverage and system reliability.

3. While dual-hop THz relaying has been studied, there is limited work on multi-relay configurations using DF protocols with ORS under realistic channel impairments like α–μ fading and pointing errors.

The main contributions of this work are outlined as follows:

1. A novel mathematical framework is developed for a multi-relay dual-hop THz communication system utilizing DF relays and an ORS scheme that selects the best relay based on instantaneous signal to noise ratio(SNR).

2. Closed-form statistical expressions for the probability density function (PDF) and cumulative distribution function (CDF) of the end-to-end SNR are derived under the effects of α–μ fading and pointing errors.

3. Exact closed-form expressions for key performance metrics are obtained, including outage probability, average SER, and ergodic capacity, based on the derived statistical functions.

4. An asymptotic performance analysis is conducted at high SNRs, from which the system's diversity gain is analytically evaluated to provide deeper insight into the reliability of the proposed setup.

5. Finally, Monte-Carlo simulations are used to verify the correctness.

2.3.2 Chapter 3

The motivations behind the work in Chapter 3 are summarized as follows:

1. High Path Loss and Short Range in THz Communication.

2. THz links are highly sensitive to blockages and misalignment, especially in indoor or dense urban settings. Establishing and maintaining robust connectivity in non-line-of-sight (NLoS) conditions remains a critical challenge

3. While multi-relay DF schemes can extend THz link coverage, they introduce higher system complexity, latency, and energy consumption, as each relay requires active processing and full-duplex capabilities—making them less scalable for dense deployment.

4. IRSs being passive and nearly power-free, provide a more scalable alternative. Deploying multiple IRSs enables intelligent signal reflection and routing, improving diversity gain without adding hardware noise or retransmission delays.

5. Most existing studies focus on single-IRS setups, while the performance potential of multi-IRS architectures in enhancing THz communication—especially in complex propagation environments—remains underexplored and motivates this investigation.

The contributions of the work in Chapter 3 are summarized as follows:

1. We propose a multi-IRS THz system with M IRS's and N reflecting elements in each IRS.

2. The closed-form expression for end-to-end CDF of the overall instantaneous SNR is derived in terms of multivariate Fox's H-function. With the help of CDF statistics, the closed-form expressions for OP, ASER and ergodic capacity are obtained in terms of multivariate Fox's H-function using Gauss-Lauguerre approximation.

3. An asymptotic performance analysis is conducted at high SNRs for outage probability(OP) and ASER, from which the system's diversity gain is obtained.

4. Monte-Carlo simulations results validate the theoretical expressions and show that increasing the number of RIS and its elements yields higher diversity gain and significantly improves reliability and SNR performance.

2.4 Organization of the Thesis

The rest of this thesis is organized as follows: In Chapter 3, Multi-Relay-Enhanced Dual-Hop Terahertz Communication system is analysed. In Chapter 4, Multi-IRS Assisted THz Communication system is analysed. Finally, Chapter 5, encompasses the thesis conclusion and outlines the future work's scope.

Chapter 3

Multi-Relay-Enhanced Dual-Hop Terahertz Communication: A Performance Analysis

3.1 Introduction

Recent years have seen remarkable progress in wireless communication technologies, with the advent of fifth-generation (5G) cellular networks representing a significant shift over prior generations. These networks enable a host of advanced applications, from extended reality (XR)—encompassing both virtual reality (VR) and augmented reality (AR)—to telemedicine, haptic technology, self-driving vehicles, aerial transportation, and human-machine interfaces. Yet, the high aspirations of 5G also introduce numerous challenges and limitations. It is expected that several automated and data-heavy processes will surpass the key performance indicators (KPIs) established for 5G [17].Certain applications, including telemedicine, autonomous driving, and haptic interfaces, necessitate prolonged data packets, elevated data transfer rates, and exceptionally reliable connections. These requirements are fundamentally at odds with the ultra-reliable low-latency communications (URLLC) strategy, which favors shorter packets [18]. Looking ahead, emergent technologies such as holographic teleportation will seek terabit-per-second (Tbps) data rates and microsecond-scale latency, capabilities beyond the design scope of current 5G networks. As a result, the progression to sixth-generation (6G) networks becomes imperative. Anticipated features of 6G include enhanced network density, supreme reliability, increased data throughput, broader

connectivity, and greater energy efficiency. Terahertz (THz) frequency bands are increasingly recognized as vital for advancing 6G cellular networks. Utilizing the THz spectrum promises to elevate 6G functionalities by offering multi-gigabit-per-second data rates, enhanced wireless bandwidth, and improved transmission security. These advantages underpin the expectation that future networks will incorporate increasingly higher frequencies, such as those within the THz range. However, despite these advantages, the THz band faces considerable developmental hurdles and environmental limitations, including severe path loss, signal fading, and challenges such as antenna misalignment and equipment flaws [19, 20]. Particularly, the pronounced path loss at THz frequencies, notable in dense urban environments, limits their transmission reach. Consequently, specialized path-loss models have been devised to effectively manage THz signal propagation.propagation [21, 22]. For instance, a ray-tracing method was applied to model short-distance THz channels [23].

A transmission model tailored for THz bands was developed to address both path loss and molecular absorption noise impacting wave propagation over short distances, as detailed in [24]. Additionally, Kokkoniemi et al. [25] proposed a model to explain path attenuation in the 275–400 GHz spectrum. Subsequent analyses of THz system performance using this model appear in [26]. It is also crucial to acknowledge the considerable impact of fading in THz signal propagation. The behavior of multipath fading within THz channels has been analyzed through Rician, Rayleigh, and Nakagami-m distribution models [27], and the presence of shadowing effects has been confirmed through empirical studies [28].

To address atmospheric turbulence and the challenges associated with long-distance communication where direct transmission paths are absent, THz systems have integrated various relaying techniques that bolster spatial diversity and reliability. Amplify-and-forward (AF) relaying is a predominant method discussed for enhancing THz communications, with single dual-hop relaying configurations having been thoroughly investigated in such networks [29]. Despite these advancements, the exploration of multi-relay THz systems, where multiple relays function either in tandem or independently to bridge the transmitter and receiver, remains in its infancy. Relay selection (RS) tactics prioritize relays based on optimal channel conditions, particularly choosing those with the highest signal-to-noise ratio (SNR) for efficient data transfer. This study delves into the outage performance of THz multi-relay systems, factoring in channel turbulence modeled by the α-μ distribution and the complications posed by nonzero boresight pointing errors and atmospheric attenuation, thereby

crafting a comprehensive model of the channel dynamics.

3.2 System Architecture

The proposed system considers a dual-hop THz communication network consisting of a source node (S), a destination node (D), and a set of N intermediate decode-and-forward (DF) relays, denoted as $\{R_1, R_2, \ldots, R_N\}$. The relays are deployed to assist communication between the source and the destination, which do not share a direct LoS path due to blockages or severe propagation losses in the THz band.

Each communication session consists of two time slots:

- In the first slot, the source node transmits the signal to all relay nodes.
- In the second slot, a single relay R_k is selected using an ORS scheme, and it forwards the decoded signal to the destination.

The selection criterion for the relay is based on the maximum instantaneous end-to-end signal-to-noise ratio (SNR), ensuring the best available path is used for transmission.

The channel between each node pair (S→R and R→D) is modeled as an independent α–μ fading channel superimposed with pointing error effects and distance-dependent path loss.

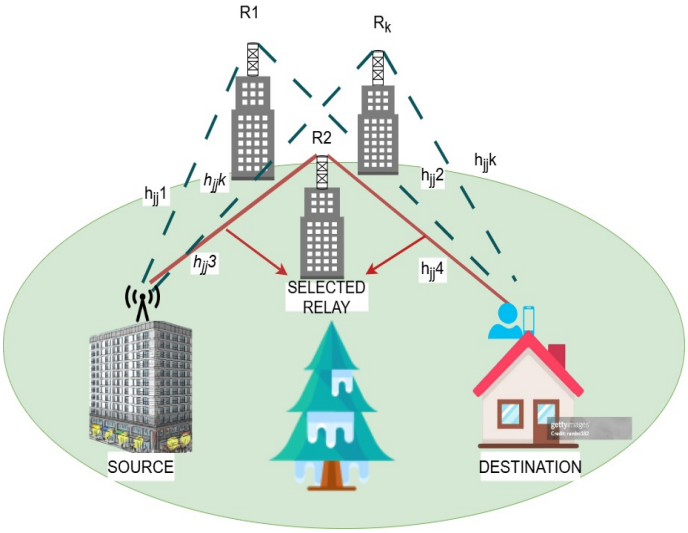

Figure 3.1: Illustration of multi-relay-based THz communication system.

3.3 Channel Model and Assumptions

We consider a multi-relay-based THz communication system as illustrated in Fig. 1. Here, two ground stations (i.e., source (S) and destination (D)) communicate through DF relaying nodes (R_k), where $k \in 1,2,...,N$. It is presumed that N aperture antennas are installed on the source and destination node which are directed toward each of the N^{th} relays, thus establishing an end-to-end THz link. These relays are equipped with two antennas each directed towards S and D.

We adopt the ORS technique [30] such that the relay-based THz link corresponding to the highest end-to-end instantaneous SNR is selected to establish a communication between S and D. As per ORS strategy, the best relay-based THz link shall be selected among N available links based on the following decision rule

$$k^{\dagger} = \arg \max_{k \in 1,2,...,N} \{\gamma_k\}, \tag{3.1}$$

where γ_k is the instantaneous SNR of the k^{th} end-to-end THz link between S and D, which can be written as [30]

$$\gamma_k = \min(\gamma_{SR_k}, \gamma_{R_kD}) \tag{3.2}$$

Note that the instantaneous SNRs of S-to-R_k and R_k-to-D links are denoted by γ_{SR_k} and γ_{R_kD}, respectively.

The combined channel gain of the THz link is given as

$$h_{jj} = h^p_{jj} h^l_{jj} h^f_{jj} \tag{3.3}$$

where $jj \in \{SR_k, R_kD\}$, h^p denotes the non-zero boresight pointing error, h^l denotes the path loss and it is taken as a deterministic quantity, and h^f denotes the multipath fading. The channel's stochastic behavior is modeled using a random process, and its PDF is given by [19]

$$|h^{fp}_{jj}| = |h^f_{jj}||h^p_{jj}| \tag{3.4}$$

The PDF of $|h^{fp}_{jj}|$ can be written as [19]

$$\begin{aligned} f_{|h^{(fp)}_{jj}|}(x) = \zeta_1^2 A_0^{-\zeta_1^2} \frac{\mu^{\frac{\zeta_1^2}{\alpha}}}{\hat{h}_f^{\alpha} \Gamma(\mu)} x^{\zeta_1^2 - 1} \\ \times \Gamma\left(\frac{\alpha\mu - \zeta_1^2}{\alpha}, \frac{\mu x^{\alpha} A_0^{-\alpha}}{\hat{h}_f^{\alpha}} \right), \end{aligned} \tag{3.5}$$

where A_0 characterizes the pointing error loss and ζ_1 represents the ratio of the equivalent beam radius to the standard deviation of the pointing error displacement at the receiver. The attenuation coefficient of the α-μ distribution is shown by the parameters α and μ. Furthermore, the gamma function is indicated by $\Gamma(\cdot)$, $\hat{h}_f$ is the α-root mean value of the fading channel envelope [31, Eq. (8.350.2)], and $\Gamma(\cdot,\cdot)$ denotes the upper incomplete gamma function [31, Eq. (8.350.2)].

The instantaneous SNR of the k^{th} THz link γ_k, is given by

$$\gamma_k = h_{jj}^{l^2} \left| h_{jj}^{fp} \right|^2 \overline{\gamma_k} \tag{3.6}$$

where $\overline{\gamma_k}$ represents the average SNR for the k^{th} THz link. Now by applying (3.6) and [19, Eq. (26)], the combined channel PDF in terms of instantaneous SNR γ_k is written as

$$\begin{aligned} f_{\gamma_k}(\gamma) = & \frac{\zeta_1^2 A_0^{-\zeta_1^2} \mu^{\frac{\zeta_1^2}{\alpha}} (h_{jj}^l)^{-\zeta_1^2}}{2\hat{h}_f^{\alpha}\Gamma(\mu)} \gamma^{\frac{\zeta_1^2}{2}-1} \overline{\gamma_k}^{-\frac{\zeta_1^2}{2}} \\ & \times \Gamma\left(\frac{\alpha\mu - \zeta_1^2}{\alpha}, \frac{\mu \gamma^{\frac{\alpha}{2}} A_0^{-\alpha}}{\hat{h}_f^{\alpha} (h_{jj}^l)^{\alpha} \overline{\gamma_k}^{\frac{\alpha}{2}}} \right) \end{aligned} \tag{3.7}$$

Based on (3.7), the CDF of γ_k is given as

$$\begin{aligned} F_{\gamma_k}(\gamma) = & 1 - \frac{\zeta_1^2 A_0^{-\zeta_1^2} \gamma^{\frac{\zeta_1^2}{2}} (h_{jj}^l)^{-\zeta_1^2}}{\hat{h}_f^{\zeta_1^2} \alpha \overline{\gamma_k}^{\frac{\zeta_1^2}{2}}} \times \\ & \sum_{k=0}^{\mu-1} \frac{\mu^{\frac{\zeta_1^2}{\alpha}}}{k!} \Gamma\left(\frac{\alpha k - \zeta_1^2}{\alpha}, \frac{\mu \gamma^{\frac{\alpha}{2}} A_0^{-\alpha}}{\hat{h}_f^{\alpha} \overline{\gamma_k}^{\frac{\alpha}{2}} (h_{jj}^l)^{-\alpha}} \right) \end{aligned} \tag{3.8}$$

By employing [32, Eq. (8.4.16.2)], (3.8) can be re-written in terms of Meijer's G-function as

$$\begin{aligned} F_{\gamma_k}(\gamma) = & \frac{2A\overline{\gamma_k}^{-\frac{\zeta_1^2}{2}} \gamma^{\frac{\zeta_1^2}{2}}}{\alpha} \times \\ & G_{2,3}^{2,1}\left[B\left(\frac{\gamma}{\overline{\gamma_k}} \right)^{\frac{\alpha}{2}} \middle| \begin{matrix} 1 - \frac{\zeta_1^2}{\alpha}, 1 \\ 0, \frac{\alpha\mu - \zeta_1^2}{\alpha}, -\frac{\zeta_1^2}{\alpha} \end{matrix} \right], \end{aligned} \tag{3.9}$$

where $A = \frac{\zeta_1^2 \mu^{\frac{\zeta_1^2}{\alpha}} (h_{jj}^l)^{\zeta_1^2}}{2\hat{h}_f^{\alpha} A_0^{\zeta_1^2} \Gamma(\mu)}$, $B = \frac{\mu}{(\hat{h}_f h_{jj}^l A_0)^{\alpha}}$, and $G_{m,n}^{p,q}[\cdot]$ is the Meijer's G-function.

3.4 Performance Evaluation

3.4.1 Outage Probability

An outage occurs in a multi-relay-based dual-hop THz communication system when the instantaneous SNR of the selected relay (i.e., the link with maximum end-to-end instantaneous SNR) falls below a certain threshold SNR γ_{th}. So, the outage probability of the proposed system is written as

$$P_{\text{out}}^{\dagger} = \Pr(\gamma_k^{\dagger} \leq \gamma_{th}) = F_{\gamma_k^{\dagger}}(\gamma_{th}), \tag{3.10}$$

where $F_{\gamma_k^{\dagger}}(\cdot)$ is the CDF expression of instantaneous SNR of the chosen relay-based THz link. Using the ORS criterion given in (3.1), $F_{\gamma_k^{\dagger}}(\gamma_{th})$ is written as

$$F_{\gamma_k^{\dagger}}(\gamma_{th}) = \Pr\left(\max_{k\in\{1,2,\ldots,N\}}\{\gamma_k\} \leq \gamma_{th}\right) = \prod_{k=1}^{N} F_{\gamma_k}(\gamma_{th}), \tag{3.11}$$

where $F_{\gamma_k}(\gamma_{th}) = \Pr(\gamma_k \leq \gamma_{th}) = \Pr(\min(\gamma_{SR_k}, \gamma_{R_kD}) \leq \gamma_{th})$. Since the intermediate links are independent of each other, $F_{\gamma_k}(\gamma_{th})$ can be re-written as

$$F_{\gamma_k}(\gamma_{th}) = 1 - \Pr(\gamma_{SR_k} > \gamma_{th}) \Pr(\gamma_{R_kD} > \gamma_{th}). \tag{3.12}$$

Thus,

$$\begin{aligned} F_{\gamma_k}(\gamma_{th}) = {} & F_{\gamma_{SR_k}}(\gamma_{th}) + F_{\gamma_{R_kD}}(\gamma_{th}) \\ & - F_{\gamma_{SR_k}}(\gamma_{th}) F_{\gamma_{R_kD}}(\gamma_{th}), \end{aligned} \tag{3.13}$$

where $F_{\gamma_{SR_k}}$ and $F_{\gamma_{R_kD}}$ are given by (3.9).

3.4.2 Average Symbol Error Rate

The ASER of the proposed system can be computed using the following expression [2]

$$\bar{P}_{\text{ser}} = \frac{t^u}{2\Gamma(u)} \int_0^{\infty} e^{-t\gamma} \gamma^{u-1} F_{\gamma_k^{\dagger}}(\gamma)\, d\gamma, \tag{3.14}$$

where t and u define the type of $M-$ary phase-shift keying (MPSK) modulation technique and its parameter values are listed in Table 4.1.

After substituting (4.6) in (4.15), we get

$$\bar{P}_{\text{ser}} = \frac{t^u}{2\Gamma(u)} \int_0^{\infty} e^{-t\gamma} \gamma^{u-1} \prod_{k=1}^{N} F_{\gamma_k}(\gamma)\, d\gamma. \tag{3.15}$$

MPSK scheme	t	u
BPSK	1	2
QPSK	2	1
8-PSK	2	0.3
16-PSK	2	0.076

Table 3.1: Modulation parameters

The integral (4.16) takes the form $\int_0^\infty e^{-x}x^n f(x)\,dx$, which can be solved using the generalized Gauss-Laguerre (GL) quadrature technique [33], and is written as

$$\bar{P}_{\text{ser}} \approx \frac{t^u}{2\Gamma(u)} \sum_{l=1}^{N} w_l f(x_l) + E_N, \tag{3.16}$$

where $f(x_l) = \prod_{k=1}^{N} F_{\gamma_k}(x_l/t)$, w_l represents the associated weight, x_l is the l-th root of the Laguerre polynomial, and E_N denotes the error term.

3.4.3 Capacity

The ergodic capacity of the multi-relay THz system is given by [33]

$$\bar{C} = \frac{1}{\ln 2} \int_0^\infty \left(1 - \frac{\prod_{k=1}^{N} F_{\gamma_k}(\gamma)}{1+\varepsilon\gamma}\right) d\gamma, \tag{3.17}$$

where $\varepsilon = 1$ and $e/2\pi$ for heterodyne detection and direct detection schemes, respectively, $F_{\gamma_k}(\gamma)$ is given by (3.13). Because of the mathematical complexity inherent in (4.10), we utilize the GL quadrature approximation to compute the ergodic capacity and the final expression is given by

$$\bar{C} \approx \frac{1}{\ln 2} \sum_{l=1}^{O} \omega_l e^{y_l} \left(1 - \frac{\prod_{k=1}^{N} F_{\gamma_k}(\gamma_l)}{1+\varepsilon\gamma_l}\right) \tag{3.18}$$

The integral can be solved using the GL quadrature method as [33]

$$\int_0^\infty f(y)\,dy \approx \sum_{l=1}^{O} w_l e^{y_l} f(y_l), \tag{3.19}$$

where O is the order of a Laguerre polynomial $L_O(y)$ and y_l is the l-th root of $L_O(y)$.

3.5 Asymptotic Analysis

In this section, the closed-form asymptotic expressions for average SER and outage probability are derived. This is accomplished by developing an asymptotic analysis of the CDF

for high SNRs, allowing $\overline{\gamma_k} \to \infty$.

3.5.1 Outage Probability

Assuming independent and identically distributed (i.i.d) fading scenario for the links between S-to-R_k and R_k-to-D, $F_{\gamma_k}(\gamma)$ given in (3.13) can be expressed as

$$F^{\infty}_{\gamma_k}(\gamma) = 2F^{\infty}_{\gamma_{SR_k}}(\gamma) - \left(F^{\infty}_{\gamma_{SR_k}}(\gamma)\right)^2 = 1 - \left(1 - F^{\infty}_{\gamma_{SR_k}}(\gamma)\right)^2. \tag{3.20}$$

After substituting (3.20) in (4.6), the asymptotic outage probability can be expressed as

$$P^{\infty}_{\text{out}} = \prod_{k=1}^{N} \left[1 - (1 - F^{\infty}_{\gamma_{SR_k}}(\gamma))^2\right], \tag{3.21}$$

where $F^{\infty}_{\gamma_{SR_k}}(\gamma)$ is the asymptotic CDF expression, which can be obtained by employing [34, Eq. (07.34.06.0040.01)] on (3.9) and the final expression is given by

$$\begin{aligned} F^{\infty}_{\gamma_{SR_k}}(\gamma) = &\frac{2A\Gamma\left(\frac{\alpha\mu-\zeta_1^2}{\alpha}\right)\Gamma\left(\frac{\zeta_1^2}{\alpha}\right)}{\alpha\Gamma\left(1+\frac{\zeta_1^2}{\alpha}\right)}\left(\frac{\gamma}{\overline{\gamma_k}}\right)^{\frac{\zeta_1^2}{2}} \\ &+\frac{2AB^{\frac{\alpha\mu-\zeta_1^2}{\alpha}}\Gamma\left(-\left(\frac{\alpha\mu-\zeta_1^2}{\alpha}\right)\right)}{\alpha\mu\Gamma\left(1-\frac{\alpha\mu-\zeta_1^2}{\alpha}\right)}\left(\frac{\gamma}{\overline{\gamma_k}}\right)^{\frac{\alpha\mu}{2}}. \end{aligned} \tag{3.22}$$

Now to obtain P^{∞}_{out}, we will substitute (3.22) in (4.13). The outage probability is asymptotically represented as

$$P^{\infty}_{\text{out}} \approx \left(G_c \cdot \overline{\gamma_k}^{-G_d}\right), \tag{3.23}$$

where G_c denotes the coding gain and G_d represents the diversity gain. Delving deeper into the asymptotic outcome for the outage probability reveals that the system's diversity gain can be readily established as $G_d = \min\left\{\frac{N\zeta_1^2}{2}, \frac{N\alpha\mu}{2}\right\}$.

It is clear that the fading parameters (α, μ), pointing error parameters (ζ_1), and number of relays N have an impact on the diversity gain of the multi-relay dual-hop THz relaying system.

3.5.2 Average Symbol Error Rate

The asymptotic average SER is obtained by substituting (3.20) in (4.16) and the final expression is given by

$$P_{\text{ser}}^{\infty} \approx \frac{t^u}{2\Gamma(u)} \sum_{l=1}^{N} \left(w_l \frac{2A\Gamma\left(\frac{\alpha\mu-\zeta_1^2}{\alpha}\right)\Gamma\left(\frac{\zeta_1^2}{\alpha}\right)}{\alpha\Gamma\left(1+\frac{\zeta_1^2}{\alpha}\right)} \left(\frac{x_l}{\overline{\gamma_k}}\right)^{\frac{\zeta_1^2}{2}} + w_l \frac{2AB^{\frac{\alpha\mu-\zeta_1^2}{\alpha}}\Gamma\left(-\frac{\alpha\mu-\zeta_1^2}{\alpha}\right)}{\alpha\mu\Gamma\left(1-\frac{\alpha\mu-\zeta_1^2}{\alpha}\right)} \left(\frac{x_l}{\overline{\gamma_k}}\right)^{\frac{\alpha\mu}{2}} \right). \tag{3.24}$$

Similar to that of asymptotic outage analysis, the diversity gain from the asymptotic average SER is obtained as $G_d = \min\left\{\frac{N\zeta_1^2}{2}, \frac{N\alpha\mu}{2}\right\}$.

3.6 Simulation Results

The analytical expressions derived in the previous section form the foundation for the numerical results presented in this section. The obtained closed-form expressions are validated through Monte Carlo simulations. We assume that the channel fading parameters (α, μ), and the pointing errors (ζ_1) are identical for both the S-to-R_k and R_k-to-D links for simplicity without loss of generality (i.e., $\alpha_1 = \alpha_2 = \alpha$, $\mu_1 = \mu_2 = \mu$, and $\zeta_{1_1} = \zeta_{1_2} = \zeta_1$). For the simulations, we set an outage threshold SNR of $\gamma_{th} = 6\,\text{dB}$. It is assumed that the relays are positioned at equal distances from both the transmitter and the receiver (i.e., $L_d = L_{do}/2$), where L_{do} represents the total transmission distance from S-to-D. The frequency of transmission and antenna gains are set to $f = 300\,\text{GHz}$ and $G_t = G_r = 55\,\text{dBi}$, respectively. We consider standard environmental conditions with relative humidity at $\rho = 50\%$, atmospheric pressure at $p_a = 101325\,\text{Pa}$, and temperature at $T = 296\,\text{K}$.

In Fig. 3.2 and 3.3, the outage probability and average SER plots are shown by varying the number of relays (i.e., $N = 1, 2, 3$) and for a link distance of $L_d = 1000$ m. In Fig. **??**(a), $N = 3$ provides an SNR gain of 2 dB and 7 dB compared to $N = 2$ and $N = 1$, respectively, to achieve an outage probability of 0.1326. Similarly in Fig. 3.3, an SNR gain of 2 dB and 8 dB is achieved by $N = 3$ when compared to $N = 2$ and $N = 1$, respectively, to achieve an average SER of 0.074. It is evident that the asymptotic results align closely with the analytical expressions for both the outage probability and average SER at high SNR levels. Furthermore, it can be observed that the outage probability decreases as N

increases. Additionally, the curves reflect consistency with the diversity order given by $G_d = \min\left\{\frac{N\zeta_1^2}{2}, \frac{N\alpha\mu}{2}\right\}$. It is also noticed that the outage probability value for $N = 3$ at an SNR of 15 dB is 10.157×10^{-3} and 0.362×10^{-3} at 20 dB. By using these values, we obtain a G_d of 2.895. For $N = 1$ at an SNR of 15 dB, the outage probability is 0.2165 and 0.0712 at 20 dB. By using these values, we obtain a G_d of 1.062. Thus, by increasing the number of relays, from $N = 1$ to $N = 3$, the diversity gain increases by 172.6%. Moreover, the simulation results closely match the analytical curves, validating the accuracy of the analytical expressions. The proposed asymptotic result also demonstrates excellent accuracy and tightness at high SNR levels.

In Fig. 3.4, we have plotted the average SER for MPSK modulation schemes, by keeping $N = 2$ and $L_d = 1000$ m. The parameter values for various modulation schemes are listed in Table-4.1. It is observed that to achieve an average SER of 0.05, BPSK has an SNR gain of 5 dB, 12 dB, and 18 dB as compared to QPSK, 8-PSK, and 16-PSK, respectively. Thus, when modulation order increases, the average SER also increases as expected. Thus, as anticipated, the system performance deteriorates as modulation order M increases.

In Fig. 3.5 and 3.6, we have plotted the outage probability and average SER curves by varying the fading parameters α, μ and ζ_1^2 for $N = 3$ and $L_d = 1000$ m. In order to demonstrate differences in outage and average SER, we first varied μ while holding α and ζ_1^2 constant. Next, we varied α while maintaining μ and ζ_1^2 constant. Third, ζ_1^2 has been adjusted while α and μ remain fixed. We observe that as α, μ and ζ_1^2 increases, the slope of the outage curve and SER increases. This suggests that mild fading and small pointing errors can lead to greater diversity gain and improved performance, whereas strong fading and large pointing errors result in lower diversity gain and performance degradation.

Fig. 3.7, compares the outage performance of single-relay and multi-relay scenarios under constant fading conditions as the link distance, L_d, varies. For an outage value of 0.0248 at $L_d = 1000$ m, a multi-relay setup with $N = 2$ relays achieves an SNR gain of 12 dB compared to the single-relay setup ($N = 1$). At a shorter link distance of $L_d = 500$ m, the same outage value of 0.0248 yields an SNR gain of 5 dB for $N = 2$ over $N = 1$. These results indicate that at shorter distances (e.g., 500 m), the system performs well with both single and multi-relay setups, though the multi-relay configuration provides a modest improvement. However, as L_d increases to 1000 m, the performance of the $N = 2$ system significantly surpasses that of the $N = 1$ scenario.

Fig. 3.8 depicts the normalized ergodic capacity curve by varying the numbers of relays and link distances. In this scenario, the fading parameters are set at $\alpha = 2$ and $\mu = 1$. It is evident that with an increase in N, the capacity of the systems improves. It is observed that to achieve an ergodic capacity of 1.5 bits/s/Hz, $N = 3$ has an SNR gain of 2 dB and 4 dB when compared to $N = 2$ and $N = 1$, respectively. Regarding distance, it can be seen that the ergodic capacity diminishes as the distance increases. This decline occurs because longer propagation distances result in greater path loss, which subsequently reduces capacity.

3.7 Conclusions

The performance of a multi-relay dual-hop THz communication system was examined in this work, employing the ORS technique to select the best relay with the highest SNR. The combined impact of path loss, non-zero boresight pointing errors, and fading were incorporated into the THz channel modeling. Additionally, we derived the closed-form expressions for the average SER, outage probability, and ergodic capacity and applied asymptotic calculations to the outage and SER to determine the diversity gain. The numerical results showed that adding additional relays improves the system performance significantly by increasing the diversity gain. Subsequently, through numerical analysis, it was demonstrated that the system performance improves with decrease in pointing errors, fading severity, and link distance.

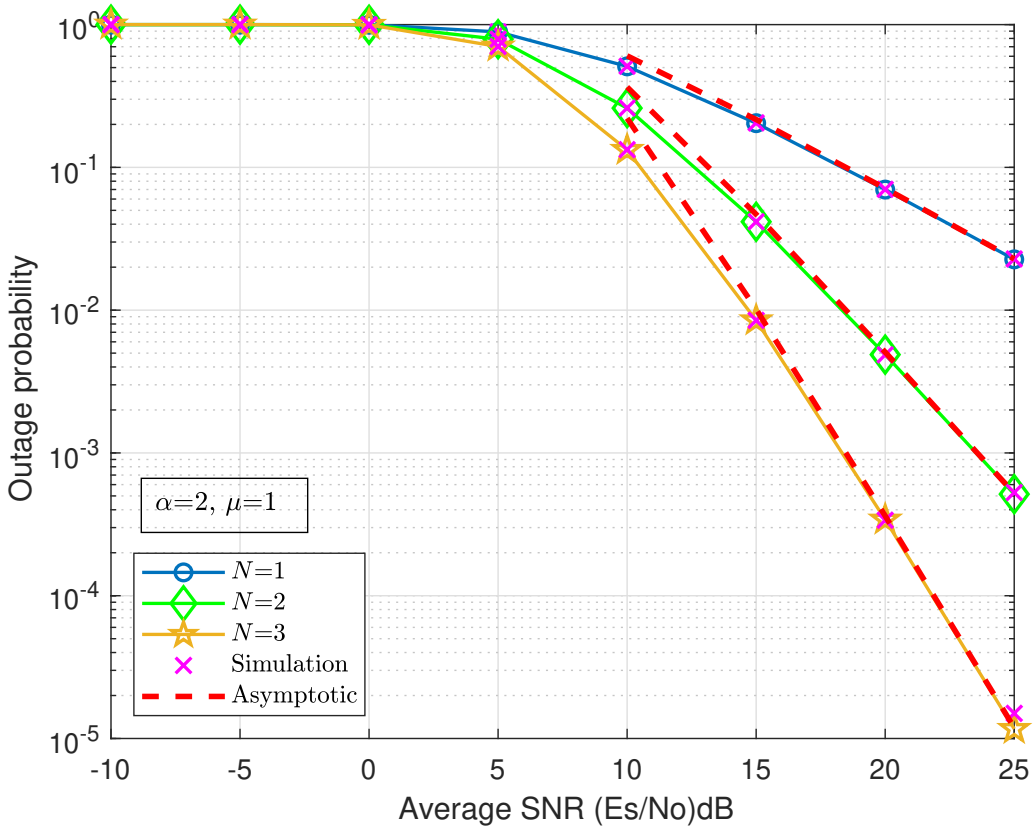

Figure 3.2: Outage performance for varying α, μ, ζ_1^2 values for N=3

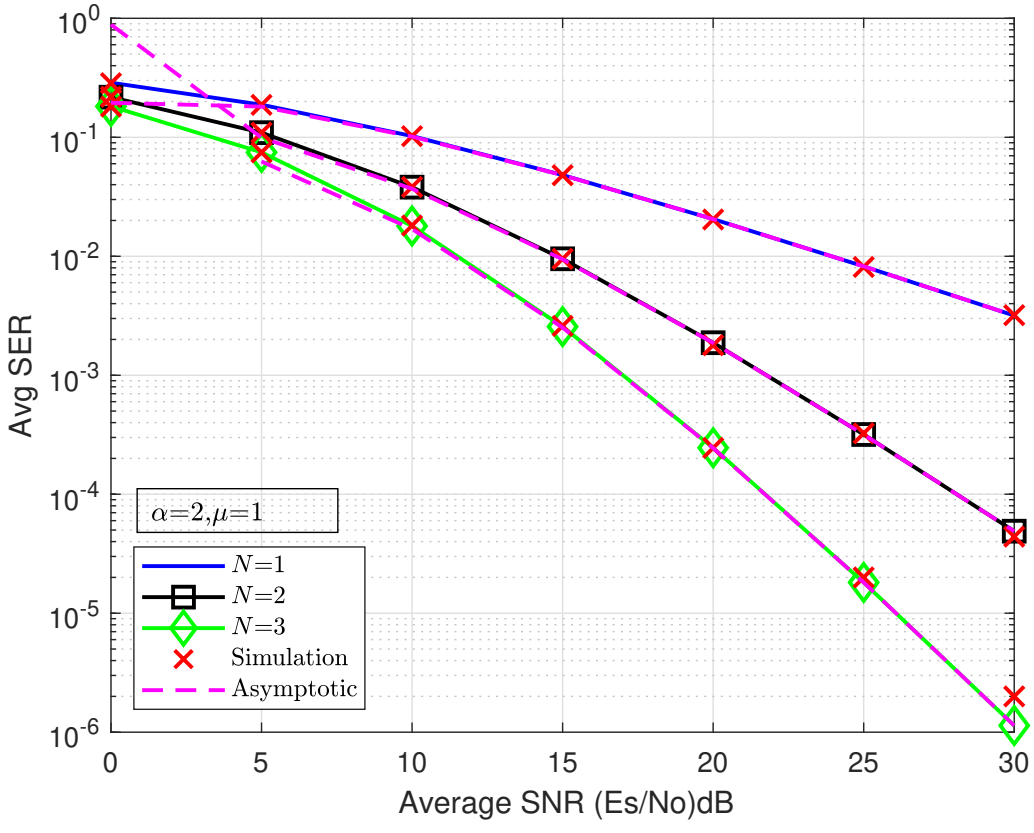

Figure 3.3: Average SER for varying α, μ, ζ_1^2 values for N=3

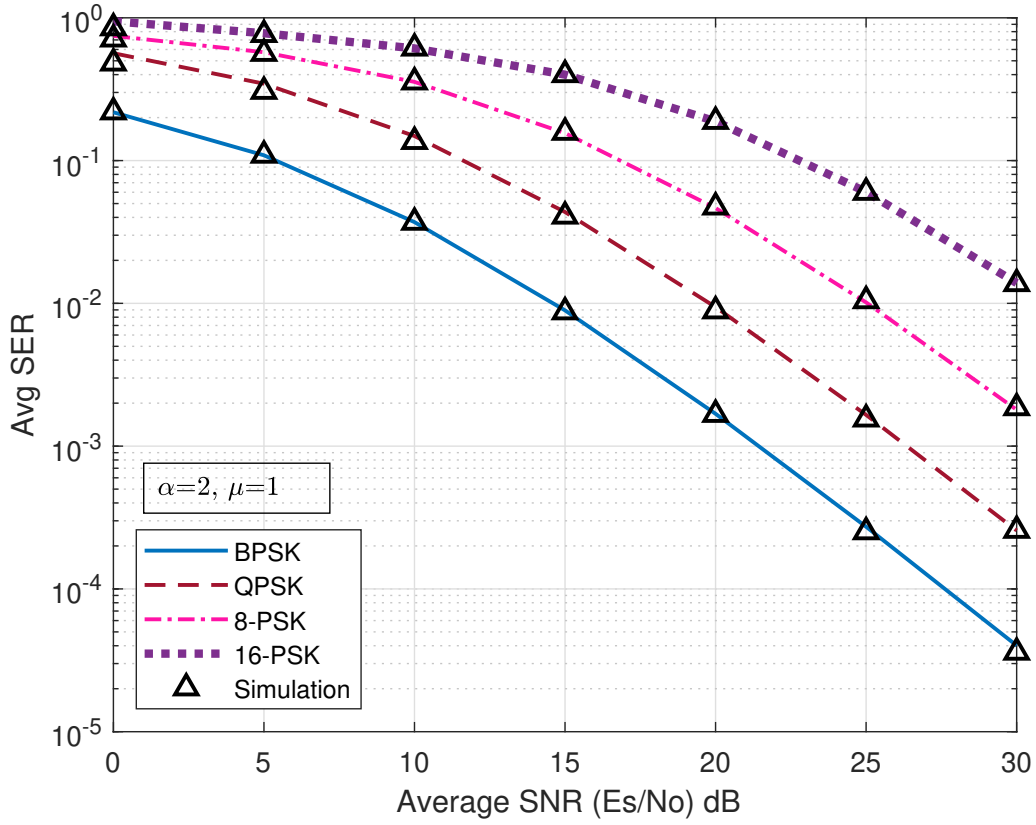

Figure 3.4: Average SER for different MPSK schemes

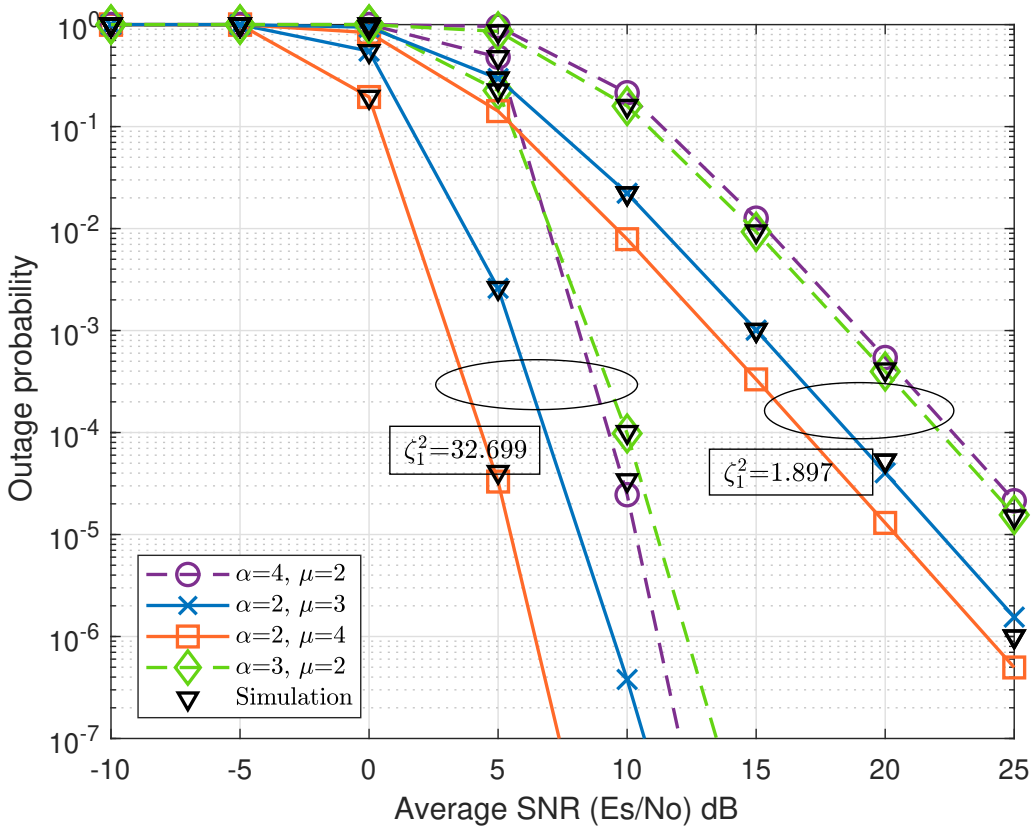

Figure 3.5: Outage performance for varying α, μ, ζ_1^2 values for N=3

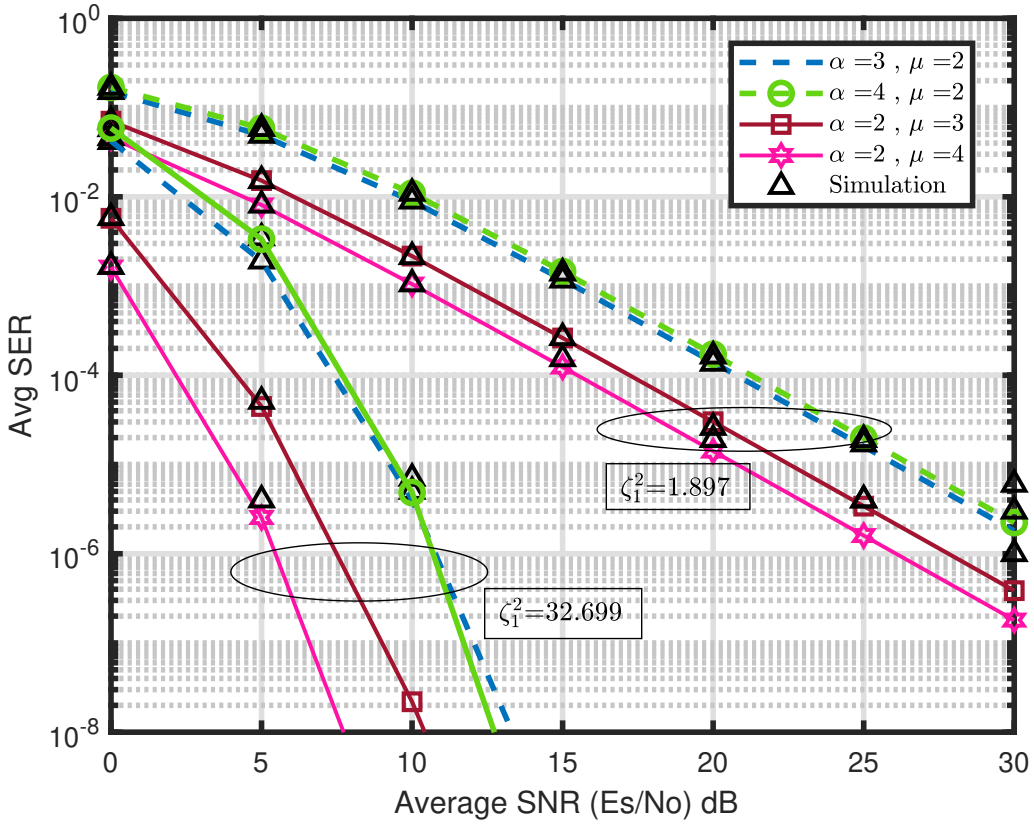

Figure 3.6: Average SER for varying α, μ, ζ_1^2 values for N=3

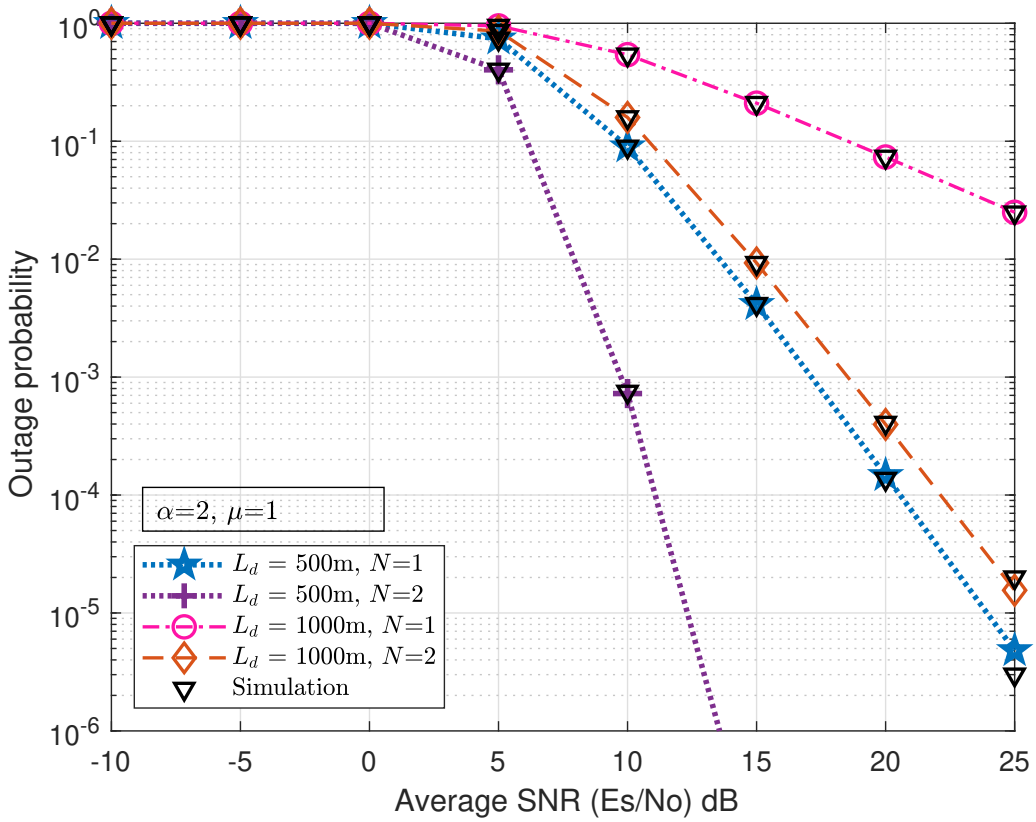

Figure 3.7: Outage probability comparison for varying L_d.

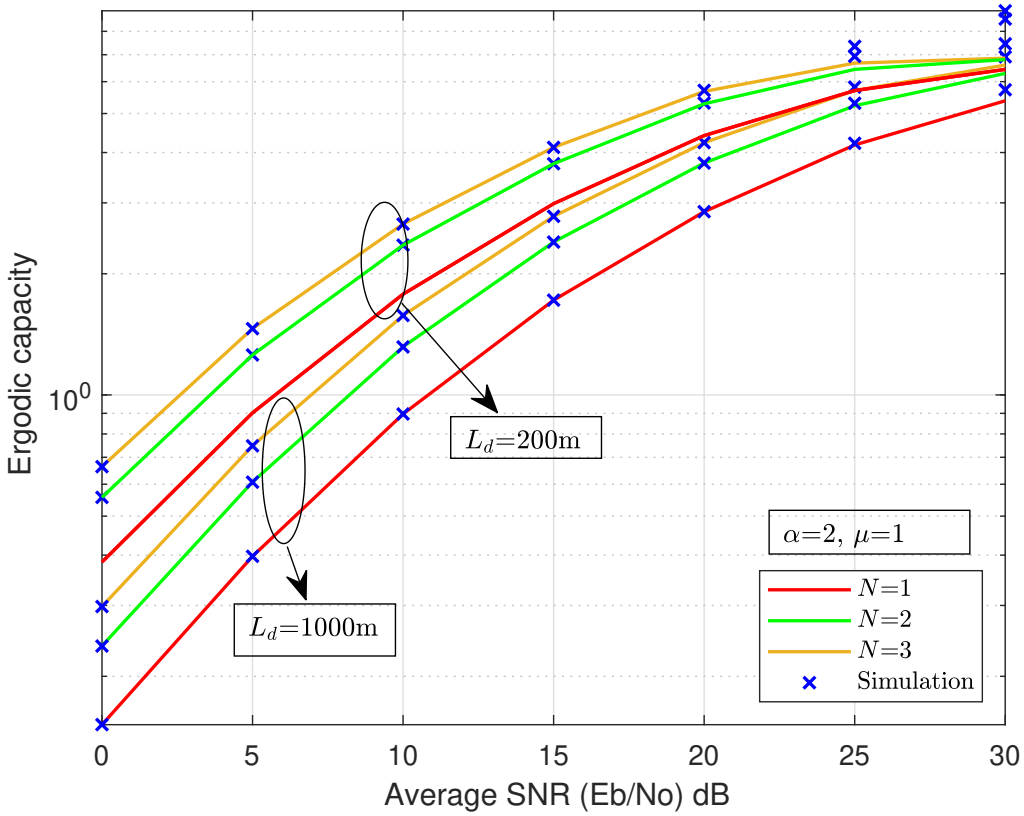

Figure 3.8: Ergodic capacity for varying N and L_d.

Chapter 4

Multi-IRS Assisted THz Communication

4.1 Introduction

Introduction

Chapter 3 explored the multi-relay-assisted dual-hop THz communication system. From that analysis, it was observed that while decode-and-forward (DF) relays help extend the communication range and improve link reliability, they introduce complexity, latency, and active power consumption. To address these limitations and further enhance system robustness in the presence of THz-specific impairments, this chapter focuses on the performance of a multi-IRS-assisted THz communication system.

The primary objective of this chapter is to investigate how multiple reconfigurable intelligent surfaces (IRSs), deployed between the source and destination, can improve signal propagation in THz environments suffering from severe path loss, molecular absorption, and pointing errors. Unlike relays, IRSs passively reflect signals and consume minimal power, making them highly suitable for dense, energy-efficient future wireless networks.

The proposed system in this chapter models a dual-hop THz setup where multiple IRSs are placed along the transmission path to create virtual line-of-sight (LoS) links. The channel is characterized using α–μ fading, combined with misalignment errors and frequency-dependent path loss to emulate realistic THz propagation.

Exact expressions for the probability density function (PDF) and cumulative distribution function (CDF) of the end-to-end signal-to-noise ratio(SNR) are derived using generalized statistical models. Using these expressions, performance metrics such as average bit error

rate (ABER), outage probability (OP), and ergodic capacity are analytically obtained. Furthermore, asymptotic analysis is also done to obtain the diversity gain. Numerical results are presented to evaluate the impact of key parameters including the number of IRS elements, and placement distance.

Finally, the analytical findings are validated through extensive Monte Carlo simulations, confirming the theoretical results and demonstrating that multi-IRS-assisted systems significantly outperform single-IRS counterparts in terms of reliability and diversity gain.

4.2 System Model

The proposed system consists of a source node (S) and a destination node (D), with no direct LoS path between them due to environmental obstructions or severe propagation losses in the THz frequency band. To enable reliable communication, the system employs a multi-IRS-assisted setup, where multiple IRS are deployed strategically between the source and destination.

Each IRS comprises a large number of passive reflecting elements capable of dynamically controlling the phase of the incident THz signal. These elements are configured to reflect the incoming signal towards the destination while enhancing the overall channel quality. The IRSs are assumed to have a fixed phase shift configuration to simplify practical implementation, effectively functioning as passive beamformers.

The system under consideration operates over a single THz communication link, which is divided into two sublinks as follows:

- **First sublink (S $\rightarrow$ IRS):** This segment connects the source node to the IRS.
- **Second sublink (IRS $\rightarrow$ D):** This segment connects the IRS to the destination node.

The overall THz channel is modeled as a cascaded fading channel, where the received signal is determined by the combined effect of both sublinks. Each sublink is characterized by the following key channel impairments:

- This statistical model captures the multipath propagation characteristics commonly observed in THz channels.
- These are introduced by a non-zero boresight radial displacement, accounting for misalignment between narrow-beam THz transceivers and the IRS elements.

- This includes path loss, which are particularly significant in the THz frequency range.

The multi-IRS configuration allows the deployment of several such surfaces along different spatial paths, providing multiple reflected LoS-equivalent paths to the destination. This setup increases the system's diversity gain and mitigates the impact of blockage or misalignment on any single path.

The mathematical modeling includes the derivation of PDF, CDF, and moment generating functions (MGF) of the end-to-end SNR, expressed using advanced tools such as Fox's H-functions. These expressions are further used to evaluate performance metrics like ABER, OP, and ergodic capacity providing a complete statistical characterization of the multi-IRS-assisted THz system.

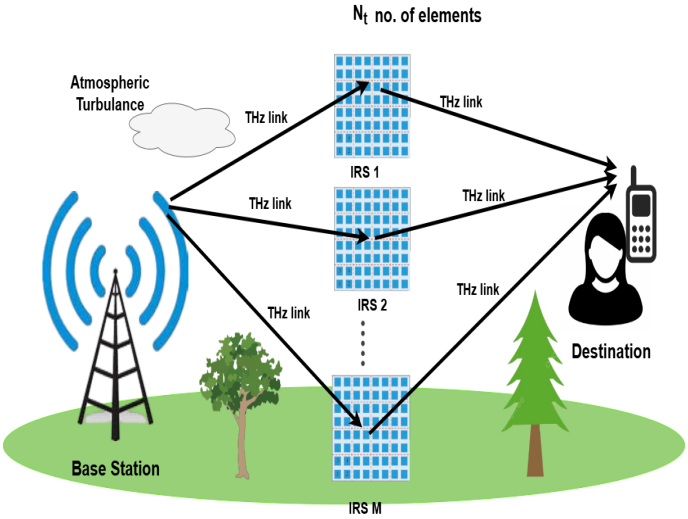

Figure 4.1: Illustration of multi-IRS assisted THz communication system.

4.3 Channel Modeling with α-μ Fading

In the IRS-assisted THz communication system, the direct LoS link between the source and the destination is assumed to be blocked. To establish reliable connectivity, M number of passive IRSs consisting of N_T reflecting elements is deployed between the source and destination. Each IRS element enables cascaded reflected path: one from the source to the IRS and the other from the IRS to the destination.

Each reflected signal path is subject to three key physical phenomena that significantly influence THz communication performance. Firstly, the small-scale fading is modeled using

the generalized α–μ distribution. This statistical model effectively captures the non-linear behavior and the multipath-rich propagation characteristics inherent in THz bands, where short wavelengths lead to rapid fluctuations in received signal strength.

Secondly, pointing errors arise due to the misalignment between the highly directional THz transceivers and the IRS surface. These errors are particularly pronounced at THz frequencies because of the narrow beamwidths, which make the system highly sensitive to even minor deviations in transceiver orientation or surface alignment. Such misalignments can cause substantial power losses and degradation in link reliability.

Lastly, path loss plays a critical role in defining the overall channel attenuation. It encompasses two dominant mechanisms: the free-space spreading loss and molecular absorption. At THz frequencies, the latter becomes especially significant due to frequency-selective absorption by atmospheric molecules, such as water vapor. The combined effect of these losses results in a frequency- and distance-dependent attenuation profile that must be carefully accounted for in system modeling.

The overall channel gain through the k-th IRS element is expressed as

$$h_k = h_{1k} \cdot h_{2k},$$

where h_{1k} and h_{2k} denote the channel gains from the source to the IRS and from the IRS to the destination, respectively. Each of these segments is modeled as an independent α–μ fading process, potentially with distinct parameters to reflect the asymmetry in geometrical layout and propagation conditions between the two sub-links.

In addition to fading, each sub-link incorporates a deterministic path loss component, given by

$$h_{Lj} = h_a \cdot h_f = \exp\left(-\frac{1}{2}\kappa_a(f_T)d_j\right) \cdot \frac{c_s\sqrt{G_T G_R}}{4\pi f_T d_j}, \quad j = 1,2,$$

where $\kappa_a(f_T)$ is the molecular absorption coefficient at the transmission frequency f_T, d_j denotes the transmission distance for the j-th sub-link (either source-to-IRS or IRS-to-destination), G_T and G_R are the antenna gains at the transmitter and receiver, respectively, and c_s represents the speed of light. This model captures the combined effects of frequency-dependent molecular attenuation and geometric spreading, which are critical to accurate performance evaluation of THz communication systems.

The pointing error is modeled using a bounded radial displacement distribution, with the coefficient depending on the beam waist, receiver aperture radius, and standard deviation of jitter.

The total channel gain of single IRS across N_T elements is the summation of cascaded channel gain of the individual elements, which is given as:

$$H = \sum_{k=1}^{N_T} h_k = \sum_{k=1}^{N_T} h_{1k} \cdot h_{2k}$$

The cascaded fading $h_{1k} \cdot h_{2k}$ results in a non-trivial distribution that lacks a simple closed-form under standard functions. Therefore, advanced mathematical tools such as the Fox's H-function are used to represent the statistical behavior of the system.

The PDF of the end-to-end SNR γ can be expressed as:

$$f_Y(x) = \frac{1}{x}\left(\prod_{d=1}^{N_t}\prod_{e=1}^{2} A_{d,e} B_{d,e}^{-\frac{\theta_{d,e}}{\alpha_{td,e}}}\right) H_{0,1:3,4;\ldots;3,4}^{0,0:4,1;\ldots;4,1}\left[\begin{array}{c|c} x\prod_{e=1}^{2} B_{1,e}^{\frac{1}{\alpha_{t1,e}}} & -:\left(v_{3k}^{(s)}, \gamma_{3k}^{(s)}\right)_{s=1:2} \\ \vdots & \\ x\prod_{e=1}^{2} B_{N_t,e}^{\frac{1}{\alpha_{tN_t,e}}} & 1;\ldots;1:\left(v_{4k}^{(s)}, \gamma_{4k}^{(s)}\right)_{s=1:4} \end{array}\right] \tag{4.1}$$

and the corresponding CDF is given by:

$$F_Y(x) = \left(\prod_{d=1}^{N_t}\prod_{e=1}^{2} A_{d,e} B_{d,e}^{-\frac{\theta_{d,e}}{\alpha_{td,e}}}\right) H_{0,1:3,4;\ldots;3,4}^{0,0:4,1;\ldots;4,1}\left[\begin{array}{c|c} x\prod_{e=1}^{2} B_{1,e}^{\frac{1}{\alpha_{t1,e}}} & -:\left(v_{3k}^{(s)}, \gamma_{3k}^{(s)}\right)_{s=1:2} \\ \vdots & \\ x\prod_{e=1}^{2} B_{N_t,e}^{\frac{1}{\alpha_{tN_t,e}}} & 0;\ldots;1:\left(v_{4k}^{(s)}, \gamma_{4k}^{(s)}\right)_{s=1:4} \end{array}\right] \tag{4.2}$$

where,

$$\left(v_{3k}^{(s)}, \gamma_{3k}^{(s)}\right)_{s=1:2} = \left[\left(1+\frac{\xi_{T1k}^2}{\alpha_{T1k}}, \frac{1}{\alpha_{T1k}}\right), \left(1+\frac{\xi_{T2k}^2}{\alpha_{T2k}}, \frac{1}{\alpha_{T2k}}\right)\right]$$

$$\left(v_{4k}^{(s)}, \gamma_{4k}^{(s)}\right)_{s=1:4} = \left[\left(\frac{\xi_{T1k}^2}{\alpha_{T1k}}, \frac{1}{\alpha_{T1k}}\right), \left(\frac{\alpha_{T1k}\mu_{1k}-1}{\alpha_{T1k}}, \frac{1}{\alpha_{T1k}}\right), \left(\frac{\xi_{T2k}^2}{\alpha_{T2k}}, \frac{1}{\alpha_{T2k}}\right), \left(\frac{\alpha_{T2k}\mu_{2k}-1}{\alpha_{T2k}}, \frac{1}{\alpha_{T2k}}\right)\right]$$

These generalized functions are essential for deriving performance metrics such as OP and ABER, and they provide an accurate and tractable way to analyze the IRS-assisted THz system under complex fading and alignment conditions.

By applying a transformation of random variables, the CDF and PDF of γ_t in terms of the distribution of Y can be derived as follows:

$$F_{\gamma_t}(\gamma) = F_Y\left(\sqrt{\frac{\gamma}{\bar{\gamma}_t y_{\text{pl}}^2}}\right) \tag{4.3}$$

$$f_{\gamma_t}(\gamma) = f_Y\left(\sqrt{\frac{\gamma}{\bar{\gamma}_t y_{\text{pl}}^2}}\right) \cdot \frac{1}{2\sqrt{\gamma\bar{\gamma}_t y_{\text{pl}}^2}} \tag{4.4}$$

where, $F_Y(\cdot)$ and $f_Y(\cdot)$ are the CDF and PDF of the random variable Y, respectively, as defined in equations (4.2) and (4.1) respectively.

4.4 Performance Metrics

4.4.1 Outage Probability

An outage occurs in a multi-IRS assisted dual-hop THz communication system when the instantaneous SNR of the selected IRS (i.e., the link with maximum end-to-end instantaneous SNR) falls below a certain threshold SNR γ_{th}. So, the OP of the proposed system is written as

$$P_{\text{out}}^{\dagger} = \Pr(\gamma_k^{\dagger} \leq \gamma_{th}) = F_{\gamma_k^{\dagger}}(\gamma_{th}), \tag{4.5}$$

where $F_{\gamma_k^{\dagger}}(\cdot)$ is the CDF expression of instantaneous SNR of the chosen IRS-assisted THz link.

$$F_{\gamma_k^{\dagger}}(\gamma_{th}) = \Pr\left(\max_{k\in\{1,2,\ldots,N\}}\{\gamma_k\} \leq \gamma_{th}\right) = \prod_{k=1}^{M} F_{\gamma_k}(\gamma_{th}), \tag{4.6}$$

4.4.2 Average Symbol Error Rate

The ABER of the proposed system can be computed using the following expression [2]

$$\bar{P}_{\text{ser}} = \frac{t^u}{2\Gamma(u)} \int_0^{\infty} e^{-t\gamma}\gamma^{u-1} F_{\gamma_k^{\dagger}}(\gamma)\, d\gamma, \tag{4.7}$$

where t and u define the type of $M-$ary phase-shift keying (MPSK) modulation technique and its parameter values are listed in Table 4.1.

MPSK scheme	**t**	**u**
BPSK	1	2
QPSK	2	1
8-PSK	2	0.3
16-PSK	2	0.076

Table 4.1: Modulation parameters

After substituting (4.6) in (4.7), we get

$$\bar{P}_{\text{ser}} = \frac{t^u}{2\Gamma(u)} \int_0^{\infty} e^{-t\gamma} \gamma^{\mu-1} \prod_{k=1}^{M} F_{\gamma_k}(\gamma)\, d\gamma. \tag{4.8}$$

The integral (4.8) takes the form $\int_0^{\infty} e^{-x} x^n f(x)\, dx$, which can be solved using the generalized Gauss-Laguerre (GL) quadrature technique [33], and is written as

$$\bar{P}_{\text{ser}} \approx \frac{t^u}{2\Gamma(u)} \sum_{l=1}^{M} w_l f(x_l) + E_N, \tag{4.9}$$

where $f(x_l) = \prod_{k=1}^{M} F_{\gamma_k}(x_l/t)$, w_l represents the associated weight, x_l is the l-th root of the Laguerre polynomial, and E_N denotes the error term.

4.4.3 Capacity

The ergodic capacity of the multi-IRS THz system is given by [33]

$$\bar{C} = \frac{1}{\ln 2} \int_0^{\infty} \left(1 - \frac{\prod_{k=1}^{M} F_{\gamma_k}(\gamma)}{1+\varepsilon\gamma} \right) d\gamma, \tag{4.10}$$

where $\varepsilon = 1$ and $e/2\pi$ for heterodyne detection and direct detection schemes, respectively, $F_{\gamma_k}(\gamma)$ is given by (4.3). Because of the mathematical complexity inherent in (4.10), we utilize the GL quadrature approximation to compute the ergodic capacity

$$\bar{C} \approx \frac{1}{\ln 2} \sum_{l=1}^{O} \omega_l e^{y_l} \left(1 - \frac{\prod_{k=1}^{M} F_{\gamma_k}(\gamma_l)}{1+\varepsilon\gamma_l} \right) \tag{4.11}$$

4.4.4 Asymptotic Analysis

The final expressions for OP and ABER depend on the CDF of the THz channels, denoted as $F_{\gamma_k}(\gamma)$. These CDFs are expressed in terms of multivariate Fox's H-function.

By assuming the high SNR approximation, i.e., $\bar{\gamma}_t \to \infty$, the CDF expressions given in equation (4.3) can be simplified. Using this high-SNR assumption, the asymptotic forms for both the OP and ABER expressions can be derived.

4.4.5 Outage Probability

By assuming $\bar{\gamma}_t \to \infty$ in (4.3), the dominant poles for the CDF $F_{\gamma_t}(\gamma)$ are determined as

$$\delta_{T_k} = \min\left\{ \zeta_{T1k}^2, \mu_{1k}\alpha_{T1k}, \zeta_{T2k}^2, \mu_{2k}\alpha_{T2k} \right\}, \quad \text{where } k = 1, 2, \ldots, N_T.$$

The corresponding asymptotic expression is written as:

$$F_{\gamma_k}^{\infty}(\gamma) = \left(\frac{\gamma}{\bar{\gamma}_t}\right)^{\frac{1}{2}\sum_{s=1}^{N_T}\delta_{Ts}} C_{T_k} \tag{4.12}$$

where C_{T_k} is given by

$$C_{T_k} = \frac{1}{\Gamma\left(1+\sum_{s=1}^{N_T}\delta_{T_s}\right)} \prod_{k=1}^{N_T} \left(E_{1k}^{\frac{1}{\alpha_{T1k}}} E_{2k}^{\frac{1}{\alpha_{T2k}}}\right)^{\delta_{T_k}}$$

$$\Gamma(\delta_{T_k}) \left[\frac{\prod^{4}_{\substack{m=1 \\ \upsilon_{4k}^{(m)} \neq \delta_{T_k}}} \Gamma\left(\upsilon_{4k}^{(m)} - \delta_{T_k}\Upsilon_{4k}^{(m)}\right) \prod_{n=1}^{2}\Gamma\left(1-\upsilon_{3k}^{(n)} + \delta_{T_k}\Upsilon_{3k}^{(n)}\right)}{\prod_{n=1}^{2}\Gamma\left(\upsilon_{3k}^{(n)} - \delta_{T_k}\Upsilon_{3k}^{(n)}\right)}\right]$$

After substituting (4.14) in (4.13), the asymptotic outage probability can be expressed as

$$P_{\text{out}}^{\infty} = \prod_{k=1}^{M} F_{\gamma_k}^{\infty}, \tag{4.13}$$

Now to obtain P_{out}^{∞}, we will substitute (4.13) in (4.15). The outage probability is asymptotically represented as

$$P_{\text{out}}^{\infty} \approx \left(G_c \cdot \overline{\gamma_k}^{-G_d}\right), \tag{4.14}$$

where G_c denotes the coding gain and G_d represents the diversity gain. Delving deeper into the asymptotic outcome for the outage probability reveals that the system's diversity gain can be readily established as $G_d = \frac{M}{2}\sum_{s=1}^{N_T}\delta_{T_s}$.

It is clear that the fading parameters (α, μ), pointing error parameters (ζ_1), number of IRS elements N and number of IRS M have an impact on the diversity gain of the multi-IRS assisted THz system.

4.4.6 Average Symbol Error Rate

The average SER of the proposed system can be computed using the following expression [2]

$$\bar{P}_{\text{ser}} = \frac{t^u}{2\Gamma(u)} \int_0^{\infty} e^{-t\gamma}\gamma^{\mu-1} F_{\gamma_k}^{\infty}(\gamma)\, d\gamma, \tag{4.15}$$

where t and u define the type of $M-$ary phase-shift keying (MPSK) modulation technique and its parameter values are listed in Table 4.1.

After substituting (4.13) in (4.17), we get

$$\bar{P}_{\text{ser}} = \frac{t^u}{2\Gamma(u)} \int_0^{\infty} e^{-t\gamma}\gamma^{\mu-1} \prod_{k=1}^{M} F_{\gamma_k}^{\infty}\, d\gamma. \tag{4.16}$$

The integral (4.16) takes the form $\int_0^\infty e^{-x} x^n f(x)\, dx$, which can be solved using the generalized Gauss-Laguerre (GL) quadrature technique [33], and is written as

$$\bar{P}_{\text{ser}} \approx \frac{t^u}{2\Gamma(u)} \sum_{l=1}^{M} w_l f(x_l) + E_N, \tag{4.17}$$

where $f(x_l) = \prod_{k=1}^{M} F_{\gamma_k}(x_l/t)$, w_l represents the associated weight, x_l is the l-th root of the Laguerre polynomial, and E_N denotes the error term.

4.5 Simulation Results

The analytical expressions derived in the previous section form the foundation for the numerical results presented in this section. The obtained closed-form expressions are validated through Monte-Carlo simulations. We assume that the channel fading parameters (α, μ), and the pointing errors (ζ_1) are identical for both the S-to-IRS_k and IRS_k-to-D links for simplicity without loss of generality (i.e., $\alpha_1 = \alpha_2 = \alpha$, $\mu_1 = \mu_2 = \mu$, and $\zeta_{1_1} = \zeta_{1_2} = \zeta_1$). For the simulations, we set an outage threshold SNR of $\gamma_{th} = 6\,\text{dB}$. It is assumed that the IRS's are positioned at equal distances from both the transmitter and the receiver (i.e., $D = D/2$), where D represents the total transmission distance from S-to-D. The frequency of transmission and antenna gains are set to $f = 300\,\text{GHz}$ and $G_t = G_r = 55\,\text{dBi}$, respectively. We consider standard environmental conditions with relative humidity at $\rho = 50\%$, atmospheric pressure at $p_a = 101325\,\text{Pa}$, and temperature at $T = 296\,\text{K}$.

In Fig. 4.2 and 4.3, the outage probability and average SER plots are shown by varying the number of relays (i.e., $N = 1, 2, 3$) and for a link distance of $D = 1000$ m. In Fig. 4.2, $M = 3$ provides an SNR gain of 2 dB and 6 dB compared to $M = 2$ and $M = 1$, respectively, to achieve an outage probability of 0.00553. Similarly in Fig. 4.3, to achieve an average SER of 1×10^{-3}, 20 dB average SNR is needed.As the number of IRSs increases, the system's computational complexity grows significantly. This makes it challenging to evaluate the average SER through both analytical derivations and simulations. It is evident that the asymptotic results align closely with the analytical expressions for both the OP and ABER at high SNR levels. Furthermore, it can be observed that the OP decreases as M increases. Additionally, the curves reflect consistency with the diversity order given by $G_d = \frac{M}{2} \sum_{s=1}^{N_T} \delta_{T_s}$. It is also noticed that the OP value for $M = 3$ at an SNR of 15 dB is 3.3085×10^{-7} and 1.0461×10^{-14} at 20 dB. By using these values, we obtain a G_d of 15. For $M = 1$ at an SNR

of 15 dB, the outage probability is 0.2165 and 0.0712 at 20 dB. By using these values, we obtain a G_d of 4.995. Thus, by increasing the number of IRSs, from $M = 1$ to $M = 3$, the diversity gain increases by 200%. Moreover, the simulation results closely match the analytical curves, validating the accuracy of the analytical expressions. The proposed asymptotic result also demonstrates excellent accuracy and tightness at high SNR levels.

Fig. 4.4 depicts the normalized ergodic capacity curve by varying the numbers of relays and link distances. In this scenario, the fading parameters are set at $\alpha = 2$ and $\mu = 1$. It is evident that with an increase in M, the capacity of the systems improves. To achieve an ergodic capacity of 6 bits/sec/Hz i.e., for an eMBB scenario for D=1000m, M =1 achieves at SNR of 15 dB for M=2 it is achieved at 10 dB. Regarding distance, it can be seen that the ergodic capacity diminishes as the distance increases. This decline occurs because longer propagation distances result in greater path loss, which subsequently reduces capacity.

4.6 Conclusion

The performance of a multi-IRS assisted THz communication system was examined in this work. The combined impact of path loss, non-zero boresight pointing errors, and fading were incorporated into the THz channel modeling. Additionally, we derived the closed-form expressions for the average SER, outage probability, and ergodic capacity and applied asymptotic calculations to the outage and SER to determine the diversity gain. The numerical results showed that adding IRS's improves the system performance significantly by increasing the diversity gain.

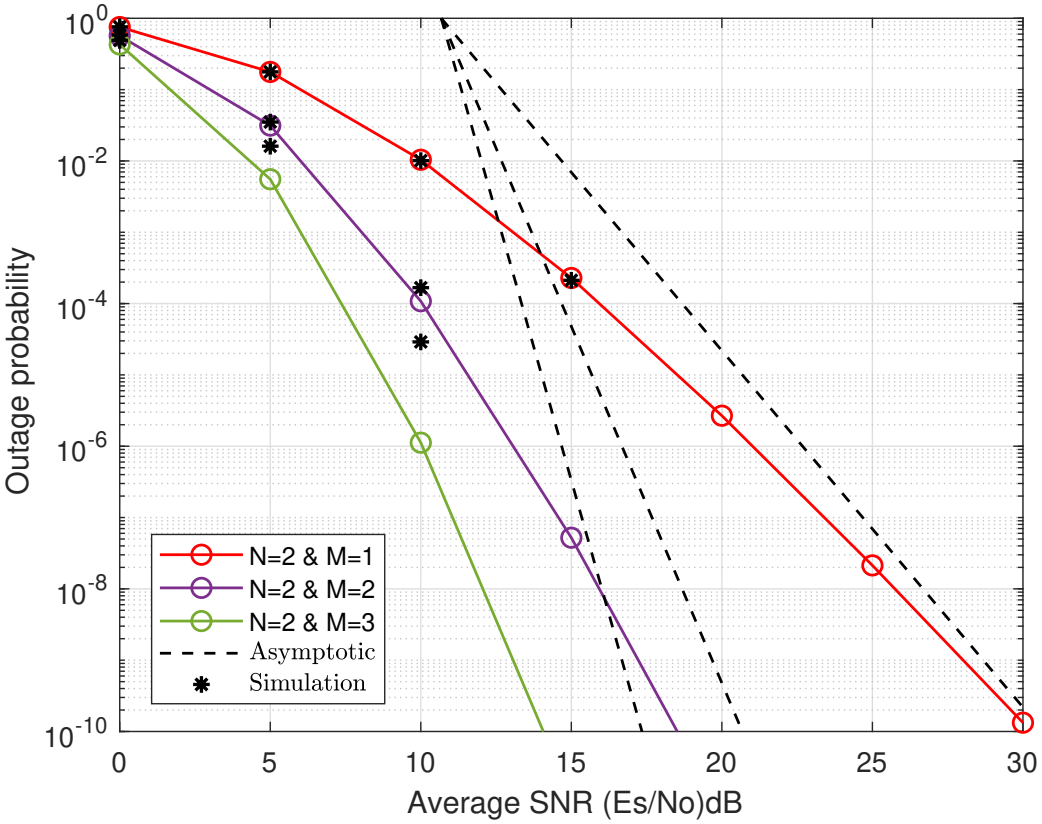

Figure 4.2: Outage performance for varying M

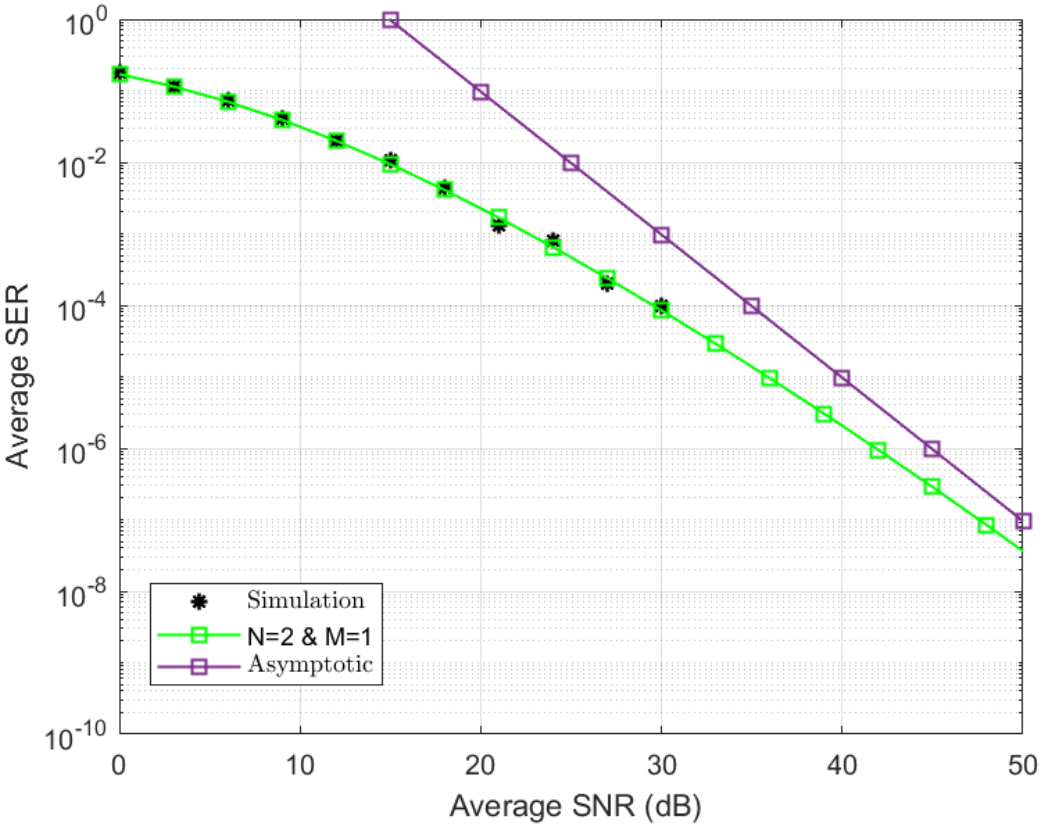

Figure 4.3: Average SER for M=1

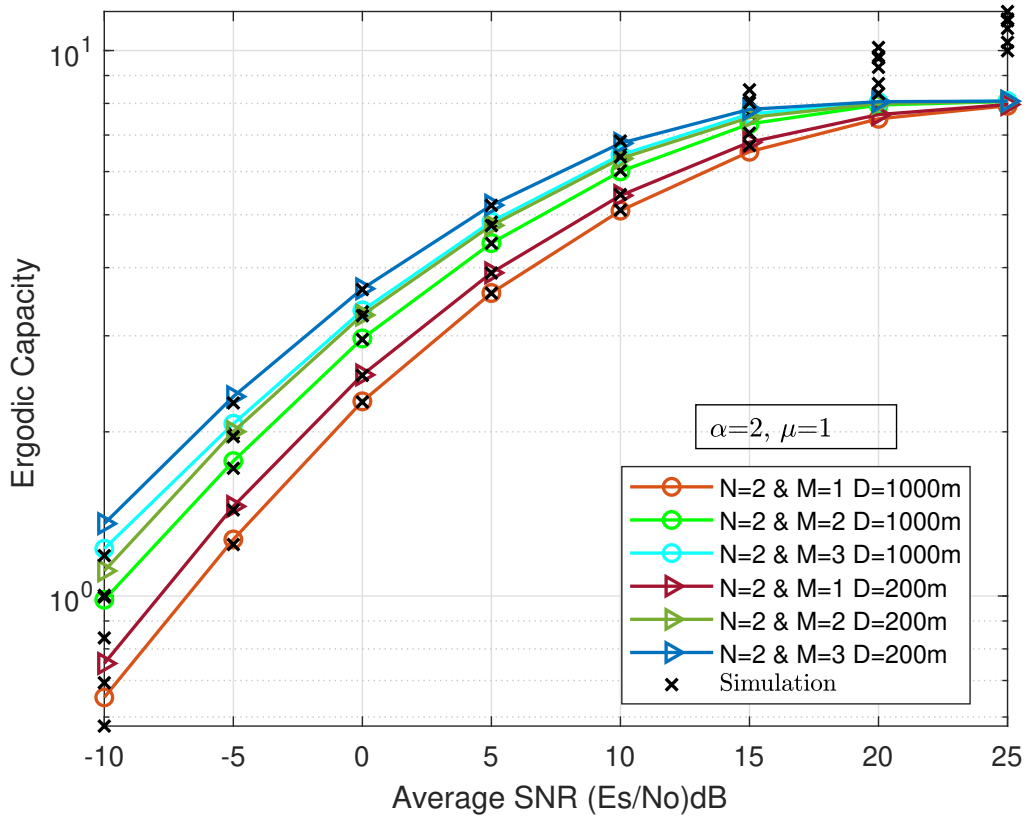

Figure 4.4: Ergodic capacity for varying M and D.

Chapter 5

Conclusions and Future Works

5.1 Conclusions

This thesis explored two promising techniques to enhance the performance and robustness of THz communication systems for future 6G networks: **multi-relay-assisted dual-hop systems** and **multi-IRS-assisted systems**.

Part I: Multi-Relay Dual-Hop THz Systems

We proposed a multi-relay THz communication framework employing DF relays with ORS. Closed-form expressions were derived for OP, ABER, and ergodic capacity under α–μ fading, distance-dependent path loss, and pointing errors. Key findings include:

- Increasing the number of DF relays significantly improves the diversity gain and reduces outage probability.
- Analytical results closely matched Monte Carlo simulations, validating the proposed models.
- Asymptotic analysis confirmed that better fading conditions and fewer pointing errors yield higher diversity gains.

Part II: Multi-IRS-Assisted THz Systems

To overcome the complexity and power consumption of relays, the second part investigated multi-IRS-assisted THz systems. These passive surfaces reconfigure the propagation environment without active power consumption. Analytical modeling using Fox's H-function provided expressions for key performance metrics. Key observations include:

- Deployment of multiple IRSs significantly improves link reliability and ergodic capacity.
- Diversity gain increases with the number of IRSs and IRS elements, enhancing performance under severe propagation impairments.
- Numerical and asymptotic results revealed tight accuracy at both moderate and high SNRs.

Overall Contributions:

- Proposed and analyzed dual-hop multi-relay and multi-IRS-assisted THz systems with realistic impairments.
- Derived closed-form and asymptotic expressions for key performance metrics using advanced mathematical tools like Meijer's G-function and multivariate Fox's H-function.
- Validated theoretical findings with comprehensive Monte Carlo simulations.

Limitations of the Work

Although the proposed systems demonstrate promising results, the analysis assumes:

- Perfect channel state information (CSI) at the transmitter, relays, and IRSs.
- Ideal IRS phase alignment and unit reflection coefficients.
- Static channel conditions and perfect synchronization.

These assumptions may not hold in practical implementations where real-time feedback, mobility, and hardware imperfections exist.

5.2 Future Works

The scope for the future work can be summarized as follows:

- All the models discussed in the thesis assumed perfect CSI conditions both at the IRS as well as at the receiver. Imperfect CSI can be explored as a part of the future work.

- For the IRS, perfect phase cancellation was assumed to maximize the SNR. As a part of future work, non-ideal conditions such as non-unity IRS reflection coefficients and imperfect phase cancellation can be considered.
- Investigation of multi-hop THz communication scenarios to overcome high path losses and extend communication range.
- Performance analysis of dual-hop transmission systems for multi-relay scenarios employing AF relaying schemes.

Conference Publications

1. Vaishali Rohilla and Swaminathan R, "*Multi Relay Enhanced Dual Hop Terahertz Communication: A Performance Analysis*", in Proceedings of the 2024 National Conference on Communication (NCC), IIT Delhi.
   Status: Accepted

Bibliography

[1] P. Bhardwaj and S. M. Zafaruddin, “Performance of Dual-Hop Relaying for THz-RF Wireless Link Over Asymmetrical α-μ Fading," in *IEEE Transactions on Vehicular Technology*, vol. 70, no. 10, pp. 10031-10047, Oct. 2021.

[2] S. Uniyal, N. Vishwakarma, and Swaminathan R, “Multi-hop IRS assisted free space optics communication with DF relaying: A performance analysis,” *Appl. Opt.*, vol. 62, pp. 4716-4726, Jun. 2023.

[3] P. Bhardwaj and S. M. Zafaruddin, “On the Performance of Multihop THz Wireless System Over Mixed Channel Fading With Shadowing and Antenna Misalignment," in *IEEE Transactions on Communications*, vol. 70, no. 11, pp. 7748-7763, Nov. 2022.

[4] I. Abadi, A. Zainudin, C. Imron and D. N. Fitriyanah, "Artificial Intelligent Based Fall Detection System for Elderly People Using IoT," 2019 International Conference on Advanced Mechatronics, Intelligent Manufacture and Industrial Automation (ICAMIMIA), Batu, Indonesia, 2019, pp. 19-24.

[5] V. K. Chapala and S. M. Zafaruddin, “Exact Analysis of RIS-Aided THz Wireless Systems Over α-μ Fading With Pointing Errors," in *IEEE Communications Letters*, vol. 25, no. 11, pp. 3508-3512, Nov. 2021

[6] A. -A. A. Boulogeorgos, E. N. Papasotiriou, J. Kokkoniemi, J. Lehtomaeki, A. Alexiou and M. Juntti, “Performance Evaluation of THz Wireless Systems Operating in 275-400 GHz Band," 2018 *IEEE 87th Vehicular Technology Conference (VTC Spring)*, Porto, Portugal, 2018, pp. 1-5

[7] N. P. Le and M.-S. Alouini, “Performance Analysis of RIS-Aided THz Communications Over α-μ Fading Channels,” *IEEE Internet Things J.*, vol. 11, no. 1, pp. 1234–1245, Jan. 2024.

[8] S. Uniyal, N. Vishwakarma, D. Singh and S. R., “Reconfigurable Intelligent Surfaces-Aided Mixed THz/FSO Communication System," 2024 *National Conference on Communications (NCC)*, Chennai, India, 2024, pp. 1-6

[9] S. Uniyal, N. Vishwakarma, D. Singh and S. R., “Reconfigurable Intelligent Surfaces-Aided Mixed THz/FSO Communication System," 2024 *National Conference on Communications (NCC)*, Chennai, India, 2024, pp. 1-6.

[10] A. Malik, V. K. Chapala, and S. M. Zafaruddin, “Performance Analysis of RIS-Assisted Vehicular Network With Direct Transmission Over Double-Generalized Gamma Fading Channels,” *J. Opt. Commun. Netw.*, vol. 14, no. 10, pp. 1234–1245, Oct. 2022.

[11] A.-A. A. Boulogeorgos, E. N. Papasotiriou, and A. Alexiou, “Performance Analysis of THz Wireless Systems in the Presence of Antenna Misalignment and Phase Noise,” *IEEE Trans. Veh. Technol.*, vol. 71, no. 4, pp. 3776–3791, Apr. 2022.

[12] H. Liu, “Computer Mathematical Modeling Based on the Improved Genetic Algorithm and Mobile Computing,” *Wireless Commun. Mob. Comput.*, vol. 2021, Article ID 5841822, 2021

[13] M. Hailat, A. A. Boulogeorgos, and A. Alexiou, “Performance Analysis of Dual-Hop Relaying for OWC System Over Foggy Channel With Pointing Errors and Atmospheric Turbulence,” *IET Commun.*, vol. 11, no. 3, pp. 1–9, 2017.

[14] H. Kaushal and G. Kaddoum, “Optical Communication in Space: Challenges and Mitigation Techniques,” *IEEE Commun. Surveys Tuts.*, vol. 19, no. 1, pp. 57–96, 2017.

[15] R. Sharma and R. Sahu, “Energy Consumption Evaluation of ZBLE, AOMDV and AODV Routing Protocols in Mobile Ad-hoc Networks,” *Ad Hoc Networks*, vol. 57, pp. 1–14, 2017.

[16] N. C. Beaulieu and J. Hu, “A Closed-Form Expression for the Outage Probability of Decode-and-Forward Relaying in Dissimilar Rayleigh Fading Channels,” *IEEE Commun. Lett.*, vol. 10, no. 12, pp. 813–815, Dec. 2006.

[17] M. Giordani, M. Polese, M. Mezzavilla, S. Rangan, and M. Zorzi, “Toward 6G networks: Use cases and technologies,” *IEEE Commun. Mag.*, vol. 58, no. 3, pp. 55–61, 2020.

[18] W. Saad, M. Bennis, and M. Chen, “A Vision of 6G wireless systems: Applications, trends, technologies, and open research problems,” *IEEE Netw.*, vol. 34, no. 3, pp. 134–142, 2020.

[19] A.-A. A. Boulogeorgos, E. N. Papasotiriou and A. Alexiou, “Analytical performance assessment of THz wireless systems," *IEEE Access*, vol. 7, pp. 11436-11453, 2019.

[20] K. Tekbiyik, A. R. Ekti, G. K. Kurt, A. Gorcin and H. Yanikomeroglu, “A holistic investigation of terahertz propagation and channel modeling toward vertical heterogeneous networks," *IEEE Commun. Mag.*, vol. 58, no. 11, pp. 14-20, November 2020.

[21] K. Tekbıyık et al., “Statistical channel modeling for short range line–of–sight terahertz communication," *in Proc. IEEE 30th Annual International Symposium on Personal, Indoor and Mobile Radio Commun. (PIMRC)*, Sep. 2019, pp. 1-5.

[22] A.-A. A. Boulogeorgos, E. N. Papasotiriou, J. Kokkoniemi, J. Lehtomaeki, A. Alexiou and M. Juntti, “Performance evaluation of THz wireless systems operating in 275-400 GHz band," *in Proc. IEEE Veh. Technol. Conf. (VTC)*, June 2018, pp. 1-5.

[23] F. Sheikh, M. El-Hadidy and T. Kaiser, “Terahertz band: Indoor ray-tracing channel model considering atmospheric attenuation," *in Proc. IEEE AP-S/URSI*, July 2015, pp. 1782-1783.

[24] F. Sheikh, N. Zarifeh, T. Kaiser, “Terahertz band: Channel modelling for short-range wireless communications in the spectral windows,” *IET Microw. Antennas Propag.*, vol. 10, no. 13, pp. 1435-1444, Oct. 2016.

[25] J. Kokkoniemi, J. Lehtomäki and M. Juntti, “Simplified molecular absorption loss model for 275–400 gigahertz frequency band," *12th Eur. Conf. Antennas Propag.(EuCAP 2018)*, London, UK, 2018, pp. 1-5.

[26] A.-A. A. Boulogeorgos, E. N. Papasotiriou, J. Kokkoniemi, J. Lehtom¨aki, A. Alexiou, and M. Juntti, “Performance evaluation of THz wireless systems operating in 275-400 GHz band,” in *Proc. IEEE Veh. Technol. Conf. (VTC)*, Jun. 2018, pp. 1-5.

[27] A. R. Ekti et al., “Statistical modeling of propagation channels for terahertz band,” in *Proc. IEEE Conf. Standards Commun. Netw. (CSCN)*, Helsinki, Finland, Sep. 2017, pp. 275-280.

[28] S. Priebe, C. Jastrow, M. Jacob, T. Kleine-Ostmann, T. Schrader, and T. Kurner, “Channel and propagation measurements at 300 GHz,” in *IEEE Trans. Antennas Propag.*, vol. 59, no. 5, pp. 1688-1698, May 2011

[29] V. U. Pai, P. Bhardwaj and S. M. Zafaruddin, "Performance Analysis of Dual-Hop THz Wireless Transmission for Backhaul Applications," in *Proc. IEEE Inte. Conf. on Advanced Networks and Telecommunications Systems (ANTS)*, Hyderabad, India, 2021, pp. 438-443.

[30] K.-S. Hwang, Y.-C. Ko, and M.-S. Alouini, “Outage probability of cooperative diversity systems with opportunistic relaying based on decode-and-forward transmission,” *IEEE Trans. Wireless Commun.*, vol. 7, no. 12, pp. 5100-5107, 2008.

[31] I. S. Gradshteyn and I. M. Ryzhic, Table of integrals, series, and products., 7th ed. San Diego, CA, USA: Academic Press, 2007.

[32] A. P. Prudnikov, Y. A. Brychkov, and O. I. Marichev, Integrals and Series: Vol. 3: More Special Functions. New York, NY, USA: CRC, 1992.

[33] S. Li, S. Yan, L. Bariah, S. Muhaidat, and A. Wang, “IRS-assisted full duplex systems over Rician and Nakagami fading channels,” *IEEE Open J. Veh. Technol.*, vol. 4, pp. 217-229, 2023.

[34] The Wolfram Functions Site. [Online]. Available: https://functions.wolfram.com/HypergeometricFunctions/MeijerG/.